Sixteen years of GOME/ERS-2 total ozone data: The new direct-fitting GOME Data Processor (GDP) version 5—Algorithm description

M. Van Roozendael,[1] R. Spurr,[2] D. Loyola,[3] C. Lerot,[1] D. Balis,[4] J.-C. Lambert,[1] W. Zimmer,[3] J. van Gent,[1] J. van Geffen,[1] M. Koukouli,[4] J. Granville,[1] A. Doicu,[3] C. Fayt,[1] and C. Zehner[5]

Received 27 June 2011; revised 18 November 2011; accepted 22 November 2011; published 9 February 2012.

[1] The Global Ozone Monitoring Instrument (GOME) was launched in April 1995 on ESA's ERS-2 platform, and the GOME Data Processor (GDP) operational retrieval algorithm has produced total ozone columns since July 1995. We report on the new GDP5 spectral fitting algorithm used to reprocess the 16-year GOME data record. Previous GDP total ozone algorithms were based on the DOAS method. In contrast, GDP5 uses a direct-fitting algorithm without high-pass filtering of radiances; there is no air mass factor conversion to vertical column amount. GDP5 includes direct radiative transfer simulation of earthshine radiances and Jacobians with respect to total ozone, albedo closure and other ancillary fitting parameters - a temperature profile shift, and amplitudes for undersampling and Ring-effect interference signals. Simulations are based on climatological ozone profiles extracted from the TOMS Version 8 database, classified by total column. GDP5 uses the high-resolution Brion-Daumont-Malicet ozone absorption cross-sections, replacing older GOME-measured flight model data. The semi-empirical molecular Ring correction developed for GDP4 has been adapted for direct fitting. Cloud preprocessing for GDP5 is done using updated versions of cloud-correction algorithms OCRA and ROCINN. The reprocessed GOME GDP5 record maintains the remarkable long-term stability of time series already achieved with GDP4. Furthermore, validation results show a clear improvement in the accuracy of the ozone product with reduced solar zenith angle and seasonal dependences, particularly in comparison with correlative observations from the ground-based network of Brewer spectrophotometers.

Citation: Van Roozendael, M., et al. (2012), Sixteen years of GOME/ERS-2 total ozone data: The new direct-fitting GOME Data Processor (GDP) version 5—Algorithm description, *J. Geophys. Res.*, *117*, D03305, doi:10.1029/2011JD016471.

1. Introduction

1.1. Historical Context

[2] A reliable and accurate long-term global ozone data record is essential to monitor the expected recovery of the ozone-layer and its relation to the ongoing climate change. Global monitoring of total ozone from satellite-borne UV (Ultra Violet) spectrometers is now entering a new phase, following the launch of second-generation sensors and the development of more accurate total ozone retrieval algorithms. The GOME (Global Ozone Monitoring Experiment) instrument was launched on board the ESA (European Space Agency) ERS-2 (European Remote-sensing Satellite) platform [*European Space Agency* (*ESA*), 1995] in April 1995. Although global coverage was lost in June 2003 due to the failure of the ERS-2 tape recorder, the quality of the measurements has been excellent, from the start of the mission through to the final ERS-2 decommissioning on 04 July 2011. The current official total ozone data product is generated via GDP (GOME Data Processor) Version 4.1, using a DOAS (Differential Optical Absorption Spectroscopy) algorithm [*Van Roozendael et al.*, 2006; *Balis et al.*, 2007a]. SCIAMACHY (SCanning Imaging Absorption SpectroMeter for Atmospheric CartograpHY) was launched in March 2002 on the ENVISAT (ENVIronmental SATellite) platform [*Bovensmann et al.*, 1999], and the official ozone product is generated by SGP (SCIAMACHY Ground Processor) Version 3.01, which is based on the GDP Version 4 algorithm; see *Lerot et al.* [2009] for an overview. The GOME-2 instrument was launched in October 2006 on board the first

[1]Belgian Institute for Space Aeronomy, Brussels, Belgium.
[2]RT Solutions, Inc., Cambridge, Massachusetts, USA.
[3]Institut für Methodik der Fernerkundung, Deutsches Zentrum für Luft- und Raumfahrt, Oberpfaffenhofen, Germany.
[4]Laboratory of Atmospheric Physics, School of Physics, Faculty of Sciences, Aristotle University of Thessaloniki, Thessaloniki, Greece.
[5]ESRIN, ESA, Frascati, Italy.

0148-0227/12/2011JD016471

EUMETSAT (EUropean Organisation for the Exploitation of METeorological SATellites) polar satellite METOP-A (METeorological OPerational satellite program) [*Munro et al.*, 2006], and the operational ozone total columns have been processed routinely using the GDP4.4 algorithm [*Loyola et al.*, 2011a].

[3] The TOMS (Total Ozone Mapping Spectrometer) total ozone record dates back to 1978, but ceased in December 2006, when contact was lost with the final instrument (EP (Earth Probe) TOMS). At NASA, the new-generation ozone sensor is the joint American/Dutch/Finnish OMI (Ozone Monitoring Instrument) [*Levelt et al.*, 2006]. Launched on the EOS-AURA platform in July 2004, OMI has been operating for 7 years. The TOMS total ozone Version 8 algorithm [*Bhartia*, 2003] has been applied successfully to OMI measurements. Both the TOMS V8 and GDP4 algorithms have achieved accuracy at the "percentage level" compared to reference ground-based measurements [*Van Roozendael et al.*, 2006].

[4] The main operational Level 2 ozone data product from GDP is the global distribution of total vertical column amounts. O_3 column retrieval from GOME has (until now) been done using DOAS algorithms, comprising spectral fitting of effective slant columns followed by AMF (Air Mass Factor) computations for conversion to vertical column amounts. Version 3.0 of the GDP algorithm was validated in 2002 and written up in 2004 [*Spurr et al.*, 2005]. Partly as a result of this validation [*Lambert et al.*, 2002] and partly from an error analysis [*Van Roozendael et al.*, 2002], it was recognized that a number of issues needed to be addressed in order to obtain an improved record of total ozone.

[5] In 2003, ESA sponsored a study on improved ozone algorithms for GOME. Three groups proposed improved DOAS-style algorithms, namely: the University of Bremen Group [*Coldewey-Egbers et al.*, 2005; *Weber et al.*, 2005], the KNMI (Royal Dutch Meteorological Institute) Group [*Eskes et al.*, 2005], and the BIRA-IASB (Belgian Institute for Space Aeronomy) group, whose GDOAS algorithm was finally selected for implementation in GDP Version 4.0 [*Van Roozendael et al.*, 2006; *Balis et al.*, 2007a].

[6] As part of the ESA study, the BIRA-IASB group also developed a new *direct fitting* algorithm called GODFIT (GOme Direct FITting), which was then selected for the next GDP upgrade to Version 5. This upgrade was completed in 2010, and the operational algorithm integrated into the UPAS (Universal Processor for UV/VIS Atmospheric Spectrometers) system at DLR. First results and a brief description of the GODFIT algorithm were presented by *Lerot et al.* [2010]. In this paper, we give a detailed description of the GODFIT algorithm as it appears in the operational GOME Data Processor version 5 (GDP5); this includes several new features. A second paper is in preparation in which a validation and accuracy assessment for the 16-year record of GOME total ozone reprocessed with the GDP5 algorithm is presented.

1.2. The GOME Instrument on ERS-2

[7] The sun-synchronous polar orbiting satellite ERS-2 has a period of ~100 min and local equator crossing time of ~10h30. GOME is a nadir-viewing UV/visible spectrometer, with three forward scans (footprint 320 × 40 km^2 for 1.5-s readout) followed by a back scan, and maximum swath 960 km (scan angle of ±31° at the spacecraft). In nominal configuration (i.e., before the tape recorder failure in June 2003), global coverage is achieved daily at latitudes beyond 60° and in 3 days at the equator. There is also a polar viewing mode for improved sounding of polar latitudes during springtime. GOME has 3584 spectral channels distributed over four serial-readout detectors. The wavelength range is from 240 to 793 nm, with a moderate spectral resolution of 0.2–0.4 nm. GOME carries a Pt-Ne-Cr lamp for in-flight wavelength calibration, and a diffuser plate for daily measurement of solar irradiance. GOME also carries 3 broadband Polarization Measurement Devices (PMDs) measuring light with polarization parallel to the slit, in 16 sub-footprints of 20 × 40 km^2. The PMDs' main purpose is to generate a polarization correction for Level 1 spectra, but they are also used for cloud detection. For details on the GOME instrument, refer to the User Manual [*ESA*, 1995]. GOME resolves absorption signatures of several atmospheric trace gases; retrieved species include O_3 (total columns and profiles), total columns for several trace species including NO_2, HCHO, BrO, and SO_2. Other products include the total H_2O vapor content, cloud parameter information and absorbing aerosol index. The GOME Data Processor (GDP) has been operational since August 1996 following the GOME commissioning phase [*Loyola et al.*, 1997]. The main operational Level 2 products from GDP are global distributions of total column O_3 and NO_2.

1.3. Overview of the GDP5 Algorithm

[8] The GDP5 algorithm employs a classical inverse method of iterative least squares minimization. Heritage goes back to the analysis of ozone column measurements from the continuous-scan NIMBUS-7 data over the period 1979 to 1986 [*Joiner and Bhartia*, 1997]. GDP5 is based on a *linearized* forward model, that is, a multiple-scatter radiative transfer (RT) simulation of GOME earthshine radiances and associated weighting functions (Jacobians) with respect to state vector elements. The latter are the total O_3 column and several ancillary parameters including albedo closure coefficients, a temperature shift, amplitudes for Ring and undersampling corrections, and a wavelength registration shift. On-the-fly RT calculations are done using the LIDORT (LInearized Discrete Ordinate Radiative Transfer) model [*Spurr*, 2008]. GDP5 is a one-step algorithm, and the basic product is simpler than that for DOAS; there is no separation of slant-column fitting and AMF conversion.

[9] The flowchart in Figure 1 gives an overview of the algorithm. It is straightforward, with one major decision point. Following the initial reading of GOME radiance and irradiance data, and the input of auxiliary data (topography fields, cloud information if precalculated, optional temperature profiles), the cloud information is then derived. The latter comprises the fractional cloud cover obtained from the OCRA (Optical Cloud Recognition Algorithm) method, and the cloud top height and albedo from the ROCINN (Retrieval of Cloud Information using Neural Networks) algorithm. The iteration counter is set (n = 0), and an initial guess is made for the state vector (total ozone amount, temperature shift, closure coefficients, etc.). A unique ozone profile $P(n)$ is then constructed from the total column estimate $C(n)$, using a 1–1 column-profile map based on column-classified ozone profile climatology (in GDP5, the climatological database developed for the TOMS Version 8 total ozone retrieval

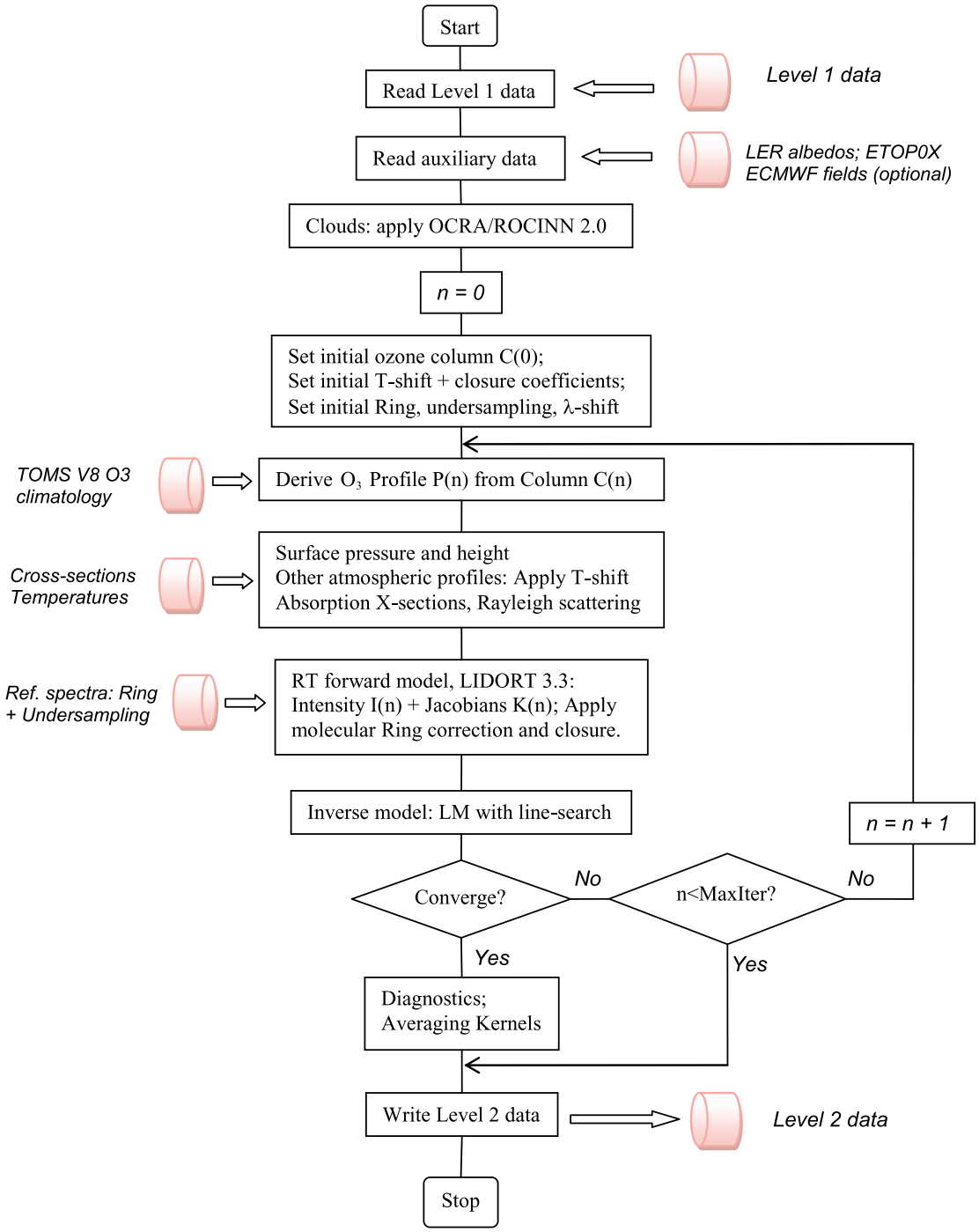

Figure 1. Flow diagram of the GDP5 direct fitting retrieval algorithm.

[*Bhartia*, 2003]). Next, pressure, temperature and height profiles are constructed; this is where the current value of the temperature shift $S(n)$ is applied. Spectral reference data are also created for the 10 nm fitting window between 325 nm and 335 nm (trace gas cross-sections, Rayleigh cross-sections and depolarization ratios).

[10] The algorithm then enters the forward model step, in which optical properties are created and the LIDORT model called to deliver top-of-atmosphere (TOA) radiances $I(n)$, and the associated ozone column, albedo, T-shift and other weighting functions $\mathbf{K}(n)$ at each iteration step n. These simulated quantities are then corrected for the molecular Ring effect. Next, the inversion module (variable-regularization Levenberg-Marquardt (LM) least squares, with line-searching) yields a new guess for the ozone column and ancillary state vector parameters. The iteration stops when suitable convergence criteria have been satisfied, or when the maximum number of iterations has been reached (in which case, there is no established convergence and final product). The O_3 total column and other parameter errors are computed directly from the inverse variance-covariance matrix.

[11] The GDP5 algorithm is described in detail in Sections 2 to 5. Section 2 describes the forward model set-up, including O_3 profile climatology, the T-shift, albedo closure terms, and trace gas cross-sections. Section 3 deals with the forward model step - generation of optical properties and simulation of radiances and Jacobians using the RT model. Section 4 describes the least squares inverse model, while Section 5 deals with ancillary algorithms (semi-empirical molecular Ring correction and cloud parameter information).

[12] Section 6 provides a quick digest of new results, including selected validations. More detailed results will be found in the sequel GDP5 validation paper (J.-C. Lambert et al., Sixteen years of GOME/ERS-2 total ozone data: The new direct-fitting GOME Data Processor (GDP) version 5: 2. Validation, manuscript in preparation, 2012). Concluding remarks are given in Section 7.

2. Forward Model Setups

2.1. Ozone Profile Climatology

[13] In a multilayer atmosphere, the forward model requires the specification of a complete ozone profile. In GDP5, the ozone profile is parameterized by a single quantity – the total column. The use of total column as a proxy for the ozone profile was recognized a number of years ago by scientists at NASA, and column-classified ozone profile climatologies were created for the TOMS Version 7 [*Wellemeyer et al.*, 1997] and Version 8 (V8) retrieval algorithms [*Bhartia*, 2003]. A TOMS-based column-profile mapping was developed for GOME AMF computations and incorporated in GDP 3.0 [*Spurr et al.*, 2005], and GDP4.0 [*Van Roozendael et al.*, 2006]. The same mapping is used for GDP5.

[14] Pressure levels defined by the TOMS V8 climatology determine the vertical layering for the forward model simulations. Pressures are halved for each successive atmospheric boundary; the scale height is 5.0 to 5.7 km. There are 12 levels corresponding to 11 'Umkehr' layers, with TOA set at 0.03 hPa. Height levels are determined by hydrostatic equilibrium based on a suitable temperature profile (see next section). In the hydrostatic balance, acceleration due to gravity varies with latitude and height according to the specification of *Bodhaine et al.* [1999]. Layering is set up for clear sky and cloudy scenes, with the lowest layer adjusted to fit the boundary pressure (surface or cloud top); height and temperature adjust linearly with the logarithm of the pressure. For each GOME footprint, we obtain surface height from the ETOP05 topographical database [*ETOP05*, 1988]. Surface pressure is either taken from analysis fields, or interpolated against the surface height using a standard atmosphere.

[15] Profiles are specified for columns at every 50 DU, for 18 latitude bands from pole to pole (10° intervals), and for each month of the year. Latitude and time variations are treated using a bilinear interpolation scheme. Columns range from 125 to 575 DU at higher latitudes down to 225 to 325 DU in the tropics. Adjustments are made to lowest Umkehr profile elements to account for the GOME scenario surface pressure or the cloud top pressure. This adjustment assumes that the partial column in any layer is proportional to the logarithm of the layer pressure drop; this is equivalent to the assumption of constant mixing ratio in a given layer.

2.2. Temperature Profiles and the T-Shift Procedure

[16] Ozone absorption in the Huggins bands is highly sensitive to temperature. Temperature profiles are required for hydrostatic balance and determination of ozone cross sections. In GDP5, temperature profiles are taken from an external source. One such source is the 10° latitude-zone 12-monthly temperature climatology supplied with the TOMS Version 8 ozone profiles [*Bhartia*, 2003]. Although more representative profiles can be obtained from meteorological analysis fields provided by the ECMWF (European Center for Medium-range Weather Forecasts) data center, it is desirable to adjust further the temperature profile to better reflect the dependence of the ozone absorption signature on temperature at the scale of GOME pixels.

[17] To this aim, an "effective temperature" is determined in DOAS algorithms as an adjustment factor from the use of two reference O_3 absorption cross sections at two different temperatures in the fitting range 325–335 nm [*Richter and Burrows*, 2002; *Van Roozendael et al.*, 2006]. In GDP5, which uses the same fitting interval as DOAS, we define a similar effective temperature T_{eff} from the input temperature profile $\{T_n\}$ through weighting with the layer ozone column amounts $\{U_n\}$: $T_{eff} \sum U_n = \sum T_n U_n$. Figure 2 (top) shows effective temperatures calculated using TOMS and ECMWF T-profiles for one GOME orbit. Figure 2 (bottom) also shows for a set of 24 GOME orbits effective temperature differences plotted against the corresponding total ozone differences. There is a remarkable linear correlation; compared with ECMWF results, a difference of 10 K in effective temperature results in a 3% change in total ozone.

[18] Figure 2 shows the importance of a reliable effective temperature to retrieve total ozone columns. Although the ECMWF temperature profiles are generally accurate, an effective temperature adjustment procedure such as in DOAS allows to further improve the total ozone product and to be less dependent from ancillary data. We now demonstrate that a temperature shift adjustment can be used in a similar way to improve total ozone accuracy in GDP5.

[19] We take an ozone profile consisting of partial columns $\{U_n\}$, $n = 1 \ldots . N_L$ (the number of layers) depending on input total column C, and a corresponding set of temperatures $\{t_n\}$ specified at associated pressure levels $\{p_n\}$, $n = 0, \ldots . N_L$. The temperature profile is given by

$$\theta_n = t_n + S\phi_n. \tag{1}$$

[20] Here, the *shift amplitude* S is treated as a free parameter to be retrieved, and ϕ_n is a prespecified *temperature shape function*. We compute column air density A_n (in [mol/cm^2]) as a two-point integration of the profile air density (in [mol/cm^3]) over the layer height thickness d_n:

$$A_n = \frac{Rd_n}{2}\left[\frac{p_{n-1}}{\theta_{n-1}} + \frac{p_n}{\theta_n}\right]. \tag{2}$$

The partial derivative of A_n with respect to the T-shift S is then given by:

$$\frac{\partial A_n}{\partial S} = -\frac{Rd_n}{2}\left[\frac{\phi_{n-1}p_{n-1}}{\theta_{n-1}^2} + \frac{\phi_n p_n}{\theta_n^2}\right]. \tag{3}$$

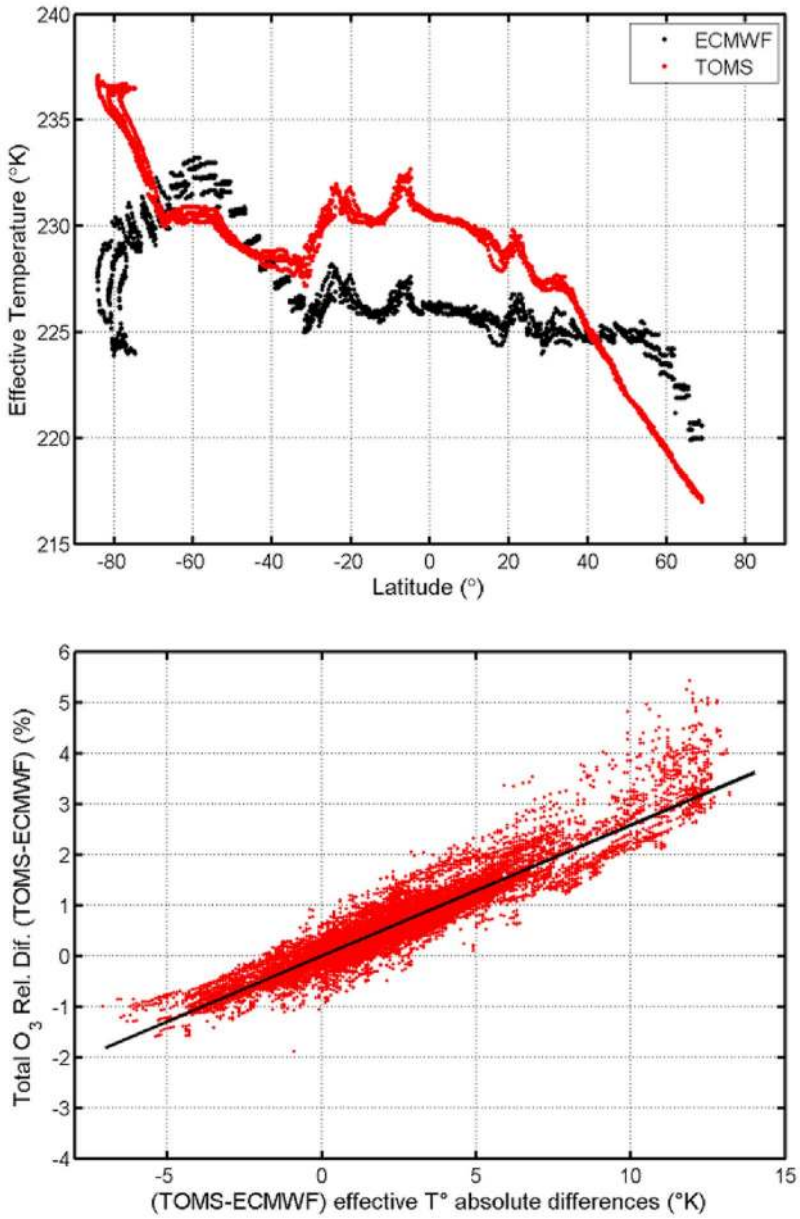

Figure 2. (top) Effective temperatures estimated from TOMS and ECMWF temperature profiles in direct fitting for GOME orbit #23802. (bottom) Total ozone relative differences plotted against effective temperature absolute differences when TOMS or ECMWF temperature profiles are used for 24 GOME orbits.

[21] Here, R is a constant proportional to Loschmidt's number. For trace gas absorption, ozone cross-sections α_n are also dependent on the T-shift S. Indeed, for a parameterized quadratic temperature dependence based on a set $\{\sigma_0, \sigma_1, \sigma_2\}$ of cross-sections, we have ($\theta^* = 273.15$ K):

$$\alpha_n = \sigma_0 + \sigma_1(\theta_n - \theta^*) + \sigma_2(\theta_n - \theta^*)^2; \quad (4)$$

$$\frac{\partial \alpha_n}{\partial S} = \phi_n[\sigma_1 + 2\sigma_2(\theta_n - \theta^*)]. \quad (5)$$

[22] Air columns and O_3 cross-sections are required for computation of optical properties input to the radiative transfer (RT) model. Since we are retrieving S, the T-shift derivatives in equations (3) and (5) will be required for linearized optical property inputs in order that the RT model generates Jacobians with respect to S. The RT setup of optical properties is discussed below in section 3.2.

[23] The default temperature shape function in GDP5 is a constant throughout the whole atmosphere; that is, $\phi_n = 1$ in all layers. However, other choices such as box or triangle functions within specified altitude ranges in the atmosphere are available. Final results were found to be weakly dependent on the actual choice of shape function, as most of the information on temperature comes from the region of ozone maximum (around 20 km altitude).

[24] In Figure 3, we present some results for the GDP5 retrieval of total ozone, with and without the T-shift parameter added to the state vector. The fitting is robust; results for 24 GOME orbits have shown that the retrieved effective temperature is virtually independent of any prescribed a priori value. In

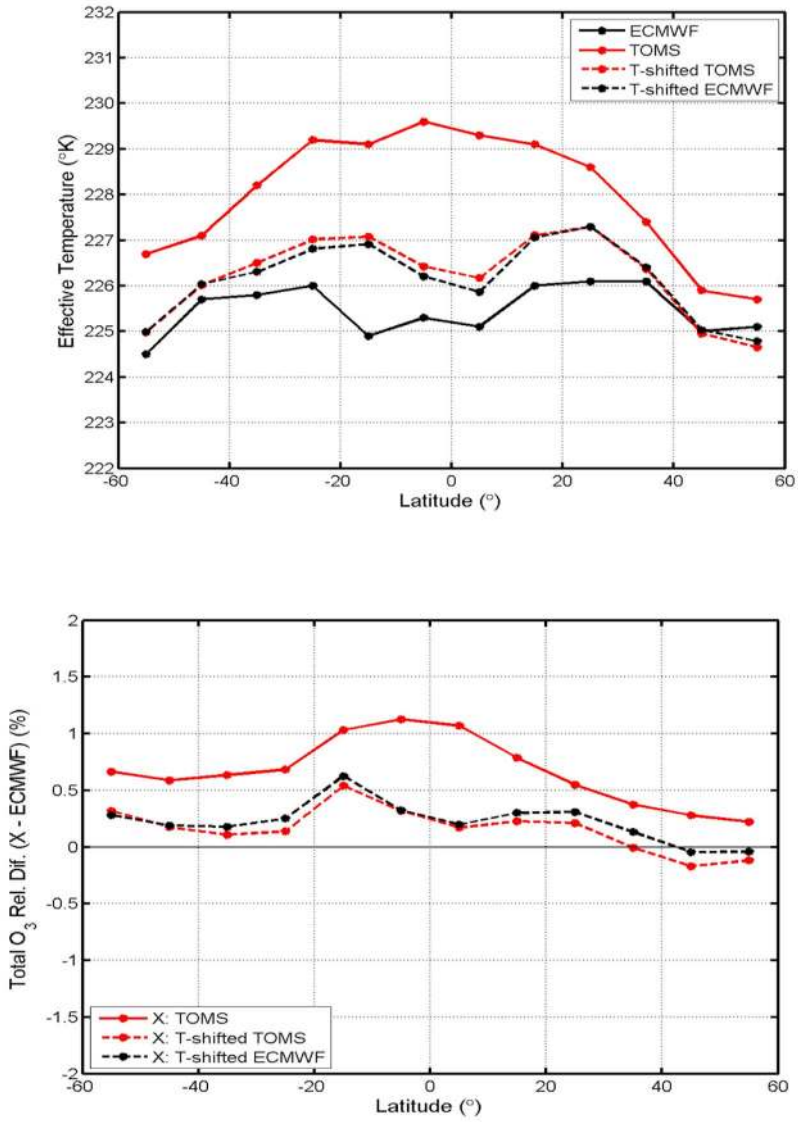

Figure 3. Illustration of the T-shift impact on retrieved total ozone columns based on 24 GOME orbits in 1999. (top) Effective temperatures retrieved using TOMS or ECMWF temperature profiles with and without T-shift. (bottom) Total ozone differences, comparing results against a non-shifted ECMWF baseline.

Figure 3 (top), effective temperatures retrieved with T-shift adjustments are close to the values derived with unshifted ECMWF temperature profiles, whereas the effective differences based on unshifted TOMS profiles are generally larger.

[25] Figure 3 (bottom) also illustrates the T-shift impact on total ozone; results with T-shifted TOMS and ECMWF temperatures are compared against a non-shifted ECMWF baseline. The observed differences are consistent with the linear relation presented in Figure 2. In general, the T-shift procedure applied to TOMS temperature profiles generally leads to small differences with respect to the ozone columns derived using ECMWF temperatures. Thus, ozone columns are consistent, no matter the choice of the a priori temperature profile. This is an important remark, as it means that the ECMWF profiles are not required as a *sine-qua-non* for accurate total columns. Consequently, GDP5 uses the climatological TOMS temperature profiles as a priori in the total ozone retrievals.

[26] Figure 4 shows the absolute differences between the DOAS and the GDP5 effective temperatures as a function of the solar zenith angle. It is clear that the DOAS temperatures are strongly biased, especially under conditions of low solar elevation. This is caused by a fundamental limitation of the DOAS approach. Indeed, the DOAS approximation (using the Beer-Lambert law) neglects the wavelength dependency of the photon path length, and this shortcoming leads to a misfit of the ozone absorption structures, which incidentally appears to be compensated by an overestimation of the effective temperature. As seen before, this has a direct impact on the retrieved total O_3 columns.

2.3. Ozone Cross-Section Data Sets

[27] For total ozone retrieval from backscatter UV sensors, the choice of ozone cross-sections has either been the older Bass/Paur laboratory data from the 1980s [*Bass and Paur*, 1984] or flight model (FM) data from GOME [*Burrows*

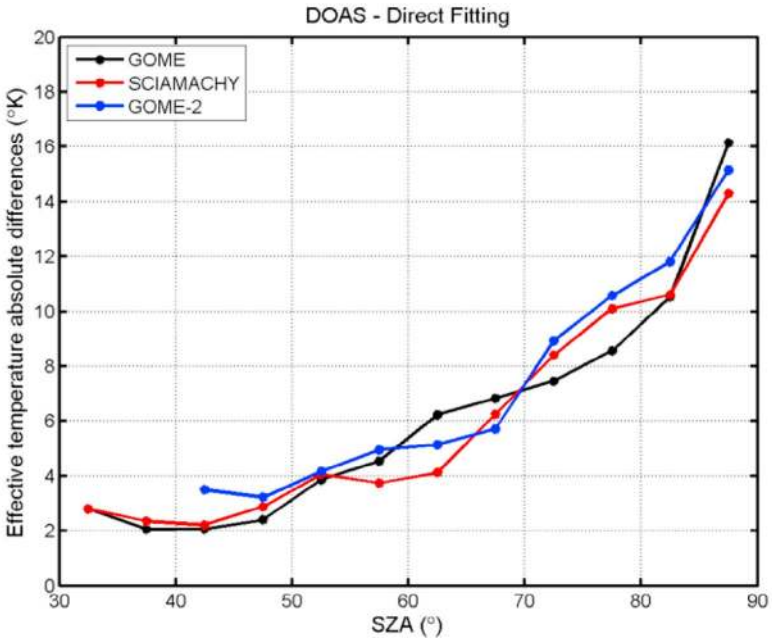

Figure 4. Mean absolute differences between the retrieved DOAS and Direct Fitting effective temperatures. The differences are plotted as a function of the solar zenith angle for three GOME, SCIAMACHY and GOME-2 orbits.

et al., 1999] or SCIAMACHY [*Bogumil et al.*, 2003]. These FM data sets are derived from measurements taken by the instruments at the preflight calibration phase. For more discussion on these data sets, see [*Orphal*, 2003]. In the Huggins bands range, the GOME baseline used re-sampled GOME FM O_3 data which included a solar I_0 correction [*Aliwell et al.*, 2002], and were preshifted (optimized preshift +0.016 nm) [see *Van Roozendael et al.*, 2006]. Cross-section uncertainty is a crucial source of retrieval error. Recently, it has become clear that newer high-resolution laboratory data (the so-called "Brion-Daumont-Malicet (BDM)" cross sections [*Daumont et al.*, 1992; *Malicet et al.*, 1995; *Brion et al.*, 1998]) give lower uncertainties than those from GOME flight model data [*Liu et al.*, 2007].

[28] These different cross-section data sets have been intercompared recently [*Lerot et al.*, 2009], highlighting large differences in terms of differential amplitudes and of wavelength calibration. The BDM data set has been recorded at high spectral resolution and can consequently be used for ozone retrievals from any space-borne UV spectrometer. In addition, this data set produces high quality fits and presents an accurate wavelength calibration. Also, its temperature dependence appears to be reliable since the retrieved effective temperatures are generally in good agreement with ECMWF temperatures (see Figure 3). For these reasons, BDM has been selected to be the reference absorption cross-section data set for GDP5 total ozone retrievals. Before use in the GDP5 retrieval scheme, the high resolution BDM cross-sections are preconvolved with predetermined GOME slit functions including a solar I_0 correction as described in GDP 4.0 [*Van Roozendael et al.*, 2006].

2.4. Albedo Closure in GDP5

[29] Scattering from tropospheric aerosol is very difficult to decouple from surface reflectivity in the UV ozone range considered here (325–335 nm). In DOAS slant column fitting, all broadband radiative effects are filtered out using a low-order polynomial. This filtering is an *external closure*; the polynomial has information on surface reflectivity variations, aerosols and cloud radiative transfer effects, and calibration inaccuracies. However, given the highly simplified forward model assumption inherent in the Beer-Lambert extinction law, it is very difficult if not impossible to extract any definitive physical interpretation from closure coefficients. In the AMF computation, aerosols are then reintroduced in an ad hoc manner; there is no real justification for this, and they become a hard-to-quantify source of error.

[30] In GDP5, it is possible to use internal or external closure for broadband signatures. For internal closure, tropospheric aerosol scattering and absorption and surface reflectivity are brought together in an *internal albedo closure term* that is fitted internally, in the sense that coupling between surface and atmosphere is treated properly in a full multiple scattering context. Direct fitting thus determines an *effective* wavelength-dependent albedo in a *molecular* atmosphere, thereby avoiding introduction of a lot of extraneous (and uncertain) aerosol information. Assuming surface albedo $R(\lambda)$ is a quadratic ($M = 2$) or cubic ($M = 3$) function of wavelength λ, we write:

$$R(\lambda) = \gamma_0 + \sum_{m=1}^{M} \gamma_m (1 - \lambda/\lambda_0)^m. \quad (6)$$

[31] This allows us to define Jacobians with respect to fitted parameters γ_0, γ_m ($m = 1,..M$):

$$K_{\gamma_o}(\lambda) = K_R(\lambda); \quad K_{\gamma_m}(\lambda) = (1 - \lambda/\lambda_0)^m K_R(\lambda). \quad (7)$$

[32] Here, $K_R(\lambda)$, is the albedo weighting function output from the radiative transfer calculation. We assume first guess values $\gamma_m = 0$ for $m > 0$, and an initial value for γ_0 is taken

from a suitable database (see below). Sensitivity results have shown that the use of albedo closure makes the algorithm insensitive to the presence of aerosols, even with absorbing aerosols in the lower troposphere.

[33] GDP5 uses the independent pixel approximation (IPA) for partially cloudy scenes. Clouds are treated as Lambertian reflectors, with cloud albedo and cloud top height derived from the ROCINN preprocessing algorithms (section 5.2). Internal closure becomes problematic for strongly cloud-contaminated scenes (cloud fraction f_c > 0.85), because of the lack of signal from the surface and lower atmosphere below cloud top. In this case we ignore any surface contributions, treating the scene as "fully cloudy mode" (f_c = 1.0) with the cloud top treated as a reflecting surface characterized by internal albedo closure. Parameter γ_0 in equation (6) is then the *retrieved* cloud top albedo.

[34] In addition, it has been shown that surface albedo closure becomes unstable under snow and ice conditions. The cloud fraction f_c delivered by the OCRA algorithm (section 5.1) is unreliable in this case, as OCRA cannot really distinguish between snow/ice and clouds. To remedy this, a "snow/ice mode" has been introduced in OCRA/ROCINN: this mode is activated when the UV surface albedo $\alpha_{UV} > 0.2$ (α_{UV} is taken from a dedicated albedo data set – see below). In this mode, f_c is set to 1.0, and cloud top albedo and cloud top height are then the retrieved "scene" albedo and height respectively. See also the discussion on the snow/ice mode in section 3.3.

[35] In GDP5, initial albedo values are specified using a dynamical albedo data set derived from accumulated satellite reflectance data. For GOME, this is the Lambertian-equivalent reflectivity (LER) data set of albedos prepared from 5.5 years of reflectivity data [*Koelemeijer et al.*, 2003]. In GDP4 and GDP5, this data is combined with Nimbus-7 TOMS LER values (N7-TOMS) prepared from 14.5 years of data from 1978 [*Herman and Celarier*, 1997], and valid for 340 and 380 nm.

[36] The GOME LER data has monthly and yearly entries on a 1° × 1° latitude/longitude grid, at 12 different wavelengths spanning the GOME range; the N7-TOMS data is also monthly. We use GOME LER data at 335 and 380 nm, and N7-TOMS LER data at 380 nm; the desired albedo is then $a(\lambda) = s(\lambda)a_{TOMS}(380)$, with scaling $s(\lambda) = a_{GOME}(\lambda)/a_{GOME}(380)$, and λ = 335 nm for ozone fitting [*Boersma et al.*, 2004]. The strengths of both data sets are combined: the long duration of the TOMS record (1978–1992) and the spectral information in the shorter GOME record (1995–2001).

[37] For activation of the snow/ice mode in OCRA/ROCINN, we use the "UV albedo" data set from *Tanskanen* [2004]. This is a global UV-range climatology with fine spatial (1° × 1°) and temporal (daily) resolution, and realistic high-latitude values. It has been created from the TOMS 360 nm reflectivity time series data (NIMBUS-7) by application of the "moving time-window" method [*Tanskanen et al.*, 2003].

3. Forward Model

3.1. Radiative Transfer

[38] In GDP5, simulation of earthshine radiances and retrieval-parameter Jacobians is done using the multilayer multiple scattering radiative transfer code LIDORT [*Spurr*, 2008, and references therein]. LIDORT generates analytic Jacobians for atmospheric and/or surface properties; the key innovation for GDP5 was the development of Jacobians for total ozone and temperature shift.

[39] LIDORT is a scalar code (no polarization) and therefore we neglect polarization in the RT modeling. However, in practice the polarization signature is subsumed in the internal closure albedo polynomial. This simplified approach is accurate enough for small fitting intervals such as used here (325–335 nm). In contrast, for the case of ozone profile retrievals, the fitting window and dynamic range are much larger; the polarization correction applied to Level 1 data is then an appreciable source of error and the inclusion of polarization in the RT simulations is necessary [see, e.g., *Liu et al.*, 2005].

[40] LIDORT solves the radiative transfer equation in each layer using the discrete-ordinate method [*Chandrasekhar*, 1960; *Stamnes et al.*, 1988]; boundary conditions (surface reflectance, level continuity, direct sunlight at top-of-atmosphere) are applied to generate the whole-atmosphere field at discrete ordinates; source function integration is then used to generate solutions at any desired viewing geometry and output level. The entire discrete ordinate RT solution is analytically differentiable with respect to any atmospheric and/or surface parameter used to construct optical properties [*Spurr*, 2002], and this allows weighting functions to be determined accurately with very little additional numerical computation, thereby avoiding finite-differencing estimation.

[41] The use of the pseudo-spherical (P-S) approximation (solar beam attenuation treated for a curved atmosphere) is standard in LIDORT; for a discussion see *Spurr* [2008]. LIDORT also has an *outgoing sphericity correction*, in which both solar and viewing angles are allowed to vary along the line-of-sight (LOS) path treated for a spherical-shell atmosphere. In general, for line-of-sight view angles not too far from zenith (∼30° or less), the regular P-S approximation gives sufficient accuracy, but for wider off-nadir viewing the outgoing sphericity correction is necessary [*Caudill et al.*, 1997; *Spurr*, 2003; *Rozanov et al.*, 2000]. Thus for regular cross-track GOME viewing (maximum swath 960 km), the P-S approximation is accurate enough, but for the GOME polar view mode [*ESA*, 1995] and for other instruments such as GOME 2 (swath 1920 km) [*Munro et al.*, 2006] and OMI [*Levelt et al.*, 2006] (swath width 2600 km), the outgoing correction is necessary.

3.2. Optical Property Setups

[42] LIDORT is a scattering code; it requires as input a set of *inherent optical properties* (IOPs). The atmosphere is assumed stratified, with a number of optically uniform layers. The IOP inputs for each layer n are $\{\Delta_n, \omega_n, \beta_{ln}\}$, comprising the total extinction optical thickness Δ_n, the total layer single scatter albedo ω_n, and the set of Legendre expansion coefficients β_{ln} for the total phase function. For Jacobian output, we need also to specify the *IOP derivatives* $\{\partial\Delta_n/\partial Q, \partial\omega_n/\partial Q, \partial\beta_{ln}/\partial Q\}$, where Q is either the total ozone column C or the T-shift S. In GDP5, the IOPs $\{\Delta_n, \omega_n, \beta_{ln}\}$ are constructed from atmospheric profiles of temperature, pressure, air density and trace gas distributions, and knowledge of Rayleigh (molecular) scattering parameters and trace gas absorption cross-sections. (Aerosol optical properties are ignored; see the discussion above.)

[43] The free atmospheric parameters are the total column C and the temperature shift S. In hydrostatic equilibrium, the air column density A_n in layer n will depend on S through equations (2) and (3). Ozone partial columns U_n depend only on C, and temperature-dependent ozone cross sections depend only on S, see equations (4) and (5). The Rayleigh scattering coefficient σ_{Ray} is determined from a standard formula (we use the formulation from *Bodhaine et al.* [1999]); there is no dependence on C and S. For $\{\Delta_n, \omega_n\}$, we write:

$$\Delta_n(C,S) = \sigma_{Ray} A_n(S) + \sigma_n^{O3}(S) U_n(C); \tag{8}$$

$$\omega_n(C,S) = \frac{\sigma_{Ray} A_n(S)}{\Delta_n(C,S)}. \tag{9}$$

[44] For molecular (Rayleigh) scattering, the phase function has a $\cos^2\Theta$ dependence on scattering angle Θ, with 3 phase function Legendre moments $\beta_0 = 1$, $\beta_1 = 0$, $\beta_2 = (1 + \rho)/(2 + \rho)$, where the depolarization ratio ρ is taken from *Chance and Spurr* [1997]. These coefficients are the same in all layers, and are independent of C and S.

[45] For the set of *linearized IOP inputs* required for LIDORT to generate Jacobians with respect to C and S, we differentiate equations (8) and (9) to find:

$$\frac{\partial \Delta_n(C,S)}{\partial C} = \sigma_n^{O3}(S) \frac{\partial U_n(C)}{\partial C}; \tag{10a}$$

$$\frac{\partial \Delta_n(C,S)}{\partial C} = \frac{\partial \sigma_n^{O3}(S)}{\partial S} U_n(C) + \sigma_{Ray} \frac{\partial A_n(S)}{\partial S}. \tag{10b}$$

$$\frac{\partial \omega_n(C,S)}{\partial C} = -\frac{\omega_n}{\Delta_n} \frac{\partial \Delta_n(C,S)}{\partial C}; \tag{11a}$$

$$\frac{\partial \omega_n(C,S)}{\partial S} = \frac{1}{\Delta_n}\left[\sigma_{Ray} \frac{\partial A_n(S)}{\partial S}\right] - \omega_n \frac{\partial \Delta_n(C,S)}{\partial S}. \tag{11b}$$

[46] In the Rayleigh-only case (no clouds/aerosols), there are no derivatives of β_{ln} (this is not the case for an atmosphere with clouds or aerosols). Linearized IOP inputs may be defined for other model parameters (such as the aerosol profile) that are sources of uncertainty in the fit; for examples appropriate to ozone profile modeling in the UV, see *van Oss and Spurr* [2002].

3.3. Surface and Cloud Setups

[47] We must specify the lower boundary reflection property for LIDORT. By default one assumes a Lambertian surface characterized by a total albedo L, but a bidirectional reflectivity formulation (BRDF) for surface reflectivity is part of the LIDORT code and can be used for sensitivity and error study. Surface albedo weighting functions have been part of LIDORT from the outset.

[48] Most ozone is above the tropopause, and in the UV, clouds are treated as a first-order correction to the basic ozone retrieval. In the independent pixel approximation (IPA), TOA radiance in a partially cloudy scenario is simulated as a linear combination of backscatter from clear and fully cloudy scenes, weighted by the *effective* cloud fractional cover f_c. Additionally, clouds are treated as Lambertian reflecting boundary surfaces. Cloud optical properties come from the OCRA/ROCINN algorithm Version 2.0 [*Loyola et al.*, 2010]. The Optical Cloud Recognition Algorithm (OCRA) provides the cloud fraction; cloud top albedo and height are obtained through ROCINN (see Section 5.2).

[49] For the partially and fully cloudy cases, part of the ozone column lies below the effective cloud top height and therefore this part may not be detected from a space-borne instrument if the optical thickness of the cloud is large enough. In DOAS applications, this missing absorption has been generally corrected by means of a "ghost column" (explicitly calculated from climatology) that is added to the column retrieved above the cloud top [see, e.g., *Spurr et al.*, 2005]. In the case of GDP5 however, a separate ghost column correction is not needed as the unique column/profile map ensures that the tropospheric part of the profile column below cloud top is implicitly adjusted in the fit (even for fully cloudy scenes).

[50] It is well known however that the use of a ghost column can lead to an overestimation of the total column when the optically thick cloud assumption is not fully satisfied [*Liu et al.*, 2004]. This may happen in particular when the cloud algorithm reports partially or fully cloudy pixels with low cloud albedo values, which effectively correspond to optically thin clouds. To minimize this effect, an empirical intracloud correction has been successfully designed for the GDP4.4 DOAS scheme [*Loyola et al.*, 2011a]. However, for GDP5, as the ghost column correction is done implicitly, the empirical intracloud correction cannot easily be applied. Therefore an alternative approach has been adopted, in which optically thin clouds retrieved by OCRA/ROCINN are transformed into equivalent optically thick clouds of reduced geometrical extent. Accordingly, effective OCRA/ROCINN parameters are defined as follows. If X is the ROCINN-derived cloud top albedo (CTA) and Y the OCRA-derived cloud fraction (CF), then effective values are:

$$CTA^* = X, \quad CF^* = Y, \quad \text{for } X > 0.8; \tag{12a}$$

$$CTA^* = 0.8, \quad CF^* = \frac{YX}{0.8}, \quad \text{for } X \le 0.8; \tag{12b}$$

[51] For scenes designated as snow- or ice-covered, the cloud algorithm cannot distinguish between ground and cloud. Thus in "ice mode," the cloud fraction is set to 1.0, and ROCINN retrieves the effective scene albedo and reflecting surface height. Because of the highly reflecting surface, the effective light path in the cloud is enhanced by multiple reflections, and there is a danger of ozone column overestimation if the ghost column is used [*Loyola et al.*, 2011a]. Likewise in GDP5, the use of a ghost column in the ice mode was abandoned.

3.4. Forward Model Closure

[52] In order to complete the forward model process, we must also account for a number of interference effects before simulated intensities can be compared with Level 1b measurements in the inverse model. The Ring effect (spectral filling-in of Fraunhofer and telluric signatures due to inelastic rotational-Raman scattering (RRS) by air molecules) shows up as small-amplitude distortions in earthshine and sky

spectra [*Grainger and Ring*, 1962]. In the ozone Huggins bands, the telluric component is significant, and the Ring effect distortion is large enough to compromise fitting accuracy. In GDP5, we use a semi-empirical determination of this signal, based on the formulation developed for the GDP4 algorithm [*Van Roozendael et al.*, 2006]; this is described in section 5.1. For this kind of Ring correction, a fitting amplitude is required for the additive Ring spectrum. An undersampling correction was introduced in GDP 3.0 to compensate for GOME's sampling slightly below the Nyquist criterion [*Slijkhuis et al.*, 1999]. The undersampling spectrum is additive; we use the GDP4 default. Thus the final sun-normalized simulated intensity may be written:

$$\frac{I(\lambda)}{I_o(\lambda)} = I_{LIDORT}(\lambda) + E_{Ring}S_{Ring}(\lambda) + E_U S_U(\lambda), \qquad (13)$$

where I_{LIDORT} is the sun-normalized intensity from LIDORT, E_{Ring} and E_U the additive amplitudes (to be determined from the fitting) for the Ring and undersampling corrections S_{Ring} and S_U respectively.

[53] In GDP5 we simulate sun-normalized radiances at wavelengths specified by the GOME solar irradiance spectrum supplied with every orbit. There is a wavelength registration mismatch between irradiance and radiance spectra, arising mainly from the solar spectrum Doppler shift; this mismatch varies across an orbit due to changes in the instrument temperature. In GDP5, an earthshine spectrum shift is fitted as part of the retrieval procedure, and this shift value is then an element in the state vector of retrieval parameters. In general, the retrieved spectrum shift value is around 0.008 nm, in line with a Doppler shift. Re-sampling is always done by cubic-spline interpolation. Note that prior to orbit processing, the wavelength registration of the solar irradiance is precisely adjusted in the 325–335 nm interval by means of a cross-correlation procedure using the highly accurate solar reference of *Chance and Kurucz* [2010]. This procedure is identical to the one thoroughly discussed by *Van Roozendael et al.* [2006] and is therefore not repeated here.

4. Inverse Model

4.1. Levenberg-Marquardt With Line-Search

[54] GDP5 is a direct fitting algorithm, using iterative nonlinear least squares minimization. In the development phase using the GODFIT prototype, the "optimal estimation" inverse method was used, with loose a priori regularization on the state vector elements. For GDP5, we have looked at alternative faster inversion codes based on Tikhonov regularization and the use of a "line-search" algorithm at each iteration step [*Doicu et al.*, 2004, 2007]. The method eventually selected for operational use in GDP5 is related to the Levenberg-Marquardt algorithm, through minimization of the following functional at the kth iteration step:

$$\mathsf{F}_k(\mathbf{x}) = \|\mathbf{F}(\mathbf{x}) - \mathbf{y}\|^2_{S_y} + \alpha_k \|\mathbf{L}_k \cdot (\mathbf{x} - \mathbf{x}_k)\|^2. \qquad (14)$$

[55] Here, we have the measurement vector of TOA radiances $\mathbf{y}_m$ (with wavelength index m), the state vector $\mathbf{x}$, the forward model simulations $\mathbf{F}(\mathbf{x})$, and the measurement error covariance matrix $\mathbf{S}_y$. $\mathbf{L}_k$ is a constant and invertible square matrix acting as a constraint, and the factor α_k is a regularization parameter which determines the strength of this constraint contribution to the functional. The forward model $\mathbf{F}(\mathbf{x})$ is linearized about its value $\mathbf{F}_k = \mathbf{F}(\mathbf{x}_k)$ according to $\mathbf{F}(\mathbf{x}) = \mathbf{F}_k + \mathbf{K}_k \cdot (\mathbf{x} - \mathbf{x}_k)$, where $\mathbf{K}_k = \mathbf{K}(\mathbf{x}_k)$ is the weighting function matrix. Setting the first derivative of the Taylor series of $\mathsf{F}_k(\mathbf{x})$ around $\mathbf{x}_k$ to zero yields the next guess:

$$\left.\begin{aligned} \mathbf{x}_{k+1} &\equiv \mathbf{x}_k + \tau_k \mathbf{p}_k = \mathbf{x}_k + \mathbf{D}_y \cdot [\mathbf{y} - \mathbf{F}_k] \\ \mathbf{D}_y &= \left[\mathbf{K}_k^{\mathrm{T}} \cdot \mathbf{S}_y^{-1} \cdot \mathbf{K}_k + \alpha_k \mathbf{L}_k^{\mathrm{T}} \cdot \mathbf{L}_k\right]^{-1} \cdot \mathbf{K}_k^{\mathrm{T}} \cdot \mathbf{S}_y^{-1} \end{aligned}\right\}. \qquad (15)$$

[56] Here, superscript T denotes matrix transpose and $\mathrm{D_y}$ is the generalized inverse or contribution function matrix. The iteration scheme of equation (15) allows us to find the search direction $\mathbf{p}_k$ (a vector with unit modulus), and the step length τ_k.

[57] Given that the functional is minimized for a certain neighborhood around $\mathbf{x}_k$ in state vector space defined by the length τ_k, we can create a group of minimum values $\mathbf{x}_i \equiv \mathbf{x}_k + \tau_i \mathbf{p}_k$ defined by a series of step lengths $\tau_i \in (0, \tau_k)$. We then search this series for a special $\mathbf{x}_j$ such that $\mathsf{F}(\mathbf{x}_j) \leq \mathsf{F}(\mathbf{x}_i), \forall i \neq j$. This is the "line-search" procedure.

[58] The line-search algorithm can produce faster convergence through fewer iterations. It can also lead to additional computational effort, since the line-search routine (and with it, the forward model) is usually called for all wavelengths in a given fitting window. However, performance gains can be achieved by application of line-search at a reduced number of wavelengths, and this was established for GDP5 by means of a sensitivity study based on 24 GOME orbits from 1999. Results from a number of trial inversion techniques and a variety of line-search wavelengths were compared with results both from the current operational GDP4.1 data and from the offline GDP5 algorithm using optimal estimation. Within the 325 to 335 nm fitting window, the "line-search" wavelengths were chosen either at equidistant spacing or at values around maxima of the Huggins bands absorption cross sections. It was found that: (1) when decreasing the number of wavelengths in the line-search algorithm, the number of calls to the forward model is lowered and the total processing time is reduced; (2) regularization with line-search can enhance speed of ozone column retrievals by up to 20% without loss of accuracy; and (3) accuracy and speed of processing depend not only on the choice of wavelengths, but also on the inversion technique applied and the use of constant or variable regularization.

[59] The sensitivity studies demonstrated that the Levenberg-Marquardt method with variable regularization (LVMR_VR) using 3 line-search wavelengths grouped closely around the 328 nm Huggins bands maximum gave the most satisfactory results. Results were identical (well within the measurement noise) to those obtained with optimal estimation, while processing time was lowered by 10–15%.

4.2. Averaging Kernel

[60] A widely used diagnostic tool that represents the sensitivity of the retrieval to the true state is the averaging kernel matrix $\mathbf{A}$. Generally speaking, it can be considered as a measure of the departure of the estimator from the truth and the dependence on any regularization settings.

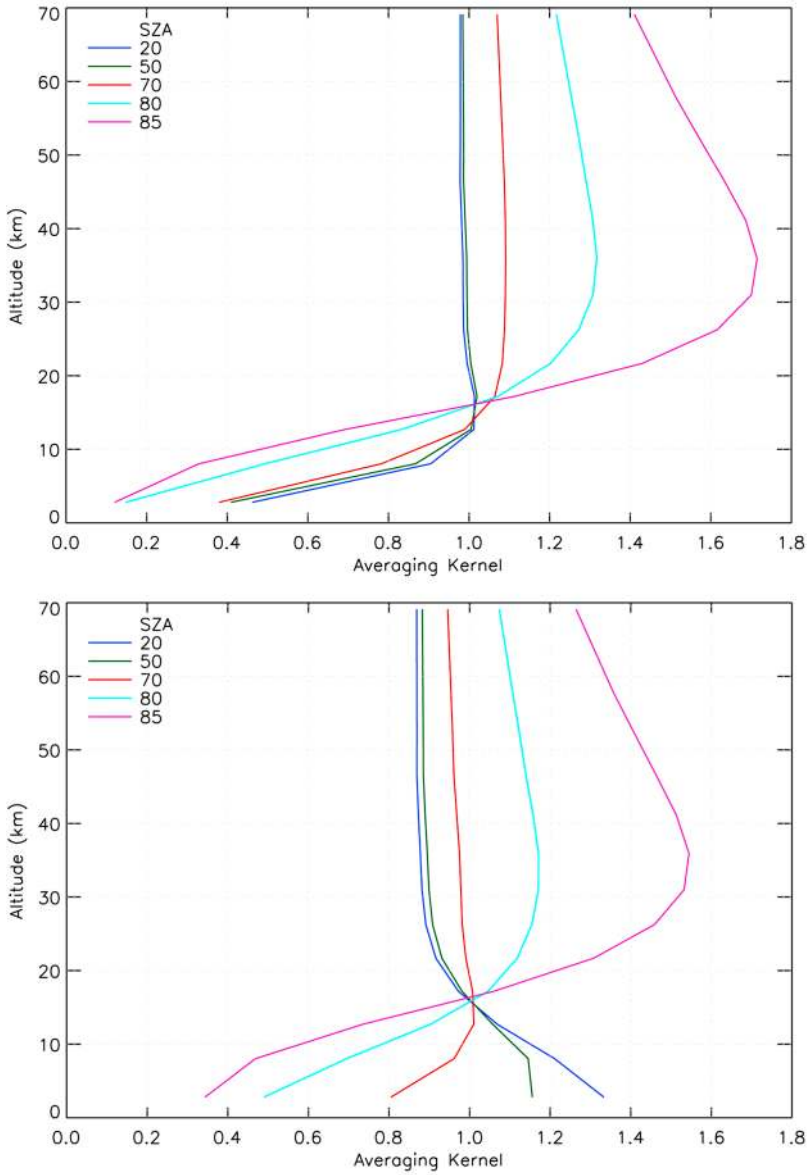

Figure 5. Column ozone averaging kernels (AK) calculated for direct nadir viewing geometry as a function of the solar zenith angle for typical midlatitude early winter ozone conditions corresponding to a total column of 350 DU. (top) Surface albedo 5%. (bottom) Surface albedo 80%.

[61] For the GDP5 total column retrieval, the problem is well-posed. Accordingly, the averaging kernel matrix reduces to a vector that indicates the sensitivity of the retrieved total column to changes in ozone concentration in different layers. It is calculated as follows. At each wavelength, the LIDORT radiative transfer model calculates the ozone profile Jacobians **K*** using that TOMS V8 ozone profile corresponding to the final retrieved total column. We then determine the contribution function matrix $\mathbf{D_y}$ from equation (15), making use of the column weighting function $\mathbf{K_i}$ calculated as part of the retrieval process. Assuming that the iteration process has converged, we can compute the averaging kernel matrix as $\mathbf{A} = \mathbf{D}_y \mathbf{K}^*$, where $\mathbf{D}_y$ is given by equation (15) with $\alpha = 0$ [e.g., *Ceccherini and Ridolfi*, 2010].

[62] Figure 5 shows averaging kernel (AK) profiles derived for typical midlatitude early winter conditions, with surface albedo 5% (Figure 5, top) and 80% (Figure 5, bottom). As can be seen, in the lowest atmospheric layers, the measurement sensitivity significantly decreases at medium and large solar zenith angles due to the reduced penetration of UV photons at low sun. For bright surface conditions typical of snow/ice scenes in Polar Regions, the sensitivity to surface ozone is considerably enhanced (Figure 5, bottom). Such profiles are generated for each GOME pixel and reported in the GDP5 data product.

4.3. State Vector and Inverse Model Settings

[63] There are 8 elements in the retrieval state vector, listed in Table 1, along with their initial value settings. Aside from total ozone, the algorithm fits the temperature-profile shift parameter, 3 polynomial coefficients for internal albedo closure, 2 amplitudes for the semi-empirical molecular Ring

Table 1. Summary of Fitting Parameters for GDP5 Direct Fitting[a]

State Vector Element Type	Number of Parameters	Initial Value
Total ozone (DU)	1	Previous-pixel
Polynomial Coefficient (Internal Closure)	3	R_{335}, 0.0, 0.0
T-shift (K)	1	0.0
Ring Fraunhofer	1	1.0
Earthshine Shift (nm)	1	0.008
Undersampling	1	0.0

[a]The total ozone first guess is taken from the previous pixel value. If this value is not available for some reason, the initial total ozone column is taken from a zonal averaged climatology based on TOMS data [*Stolarski and Frith*, 2006]. For closure, the initial value R_{335} is extracted from the surface albedo database at 335 nm as described in section 2.4; other albedo parameters are initialized to zero. Initial values of the under-sampling, earthshine λ-shift and T-shift parameters are all zero.

correction and the undersampling correction and an earthshine spectrum wavelength shift. The GOME earthshine and solar spectra are generated by the GDP Level 0-to-1b extractor [*Slijkhuis et al.*, 2004]. In addition, Level-1 wavelength calibration was improved selectively through application of window-dependent preshifts to parts of the solar spectrum [*Van Roozendael et al.*, 2006]. Preshifting of ozone cross-sections has been required to compensate for inaccuracies in the wavelength calibration of the GOME Flight Model cross-sections in GDP4 [*Van Roozendael et al.*, 2006]. However, with the use of the BDM ozone cross-sections as the new GDP5 default, it has not proved necessary to use any preshift.

[64] Although the Level 1 product has been standard for GOME for many years, there have been some recent changes which are worth noting here. In particular, Level 1b geolocation information (solar and viewing angles) is now specified at the bottom of the atmosphere (BOA), in addition to values at spacecraft and at TOA. Also newly specified is the topographic height. Second, additional cloud information from OCRA/ROCINN has been added: in addition to the cloud fraction, cloud top albedo and cloud top height (and relative errors), the product now has cloud top pressure and cloud optical thickness (the latter derived from a neural network inversion [*Loyola et al.*, 2010]), and an indication of cloud type (based on the ISCCP classification).

[65] Figure 6 displays a comparison between ozone column fitting residuals obtained using a DOAS retrieval scheme (left hand side) and the new direct-fitting scheme implemented in GDP5, for increasing values of the solar zenith angle. As can be seen, the poorly fitted ozone results typical of DOAS retrievals at low sun are strongly reduced with the direct-fitting approach. This feature is a consequence of the full physics treatment applied in GDP5.

5. Ancillary Algorithms

5.1. Molecular Ring Effect Correction

[66] In DOAS algorithms, Ring effect structures are usually dealt with by using precalculated Ring spectra, defined

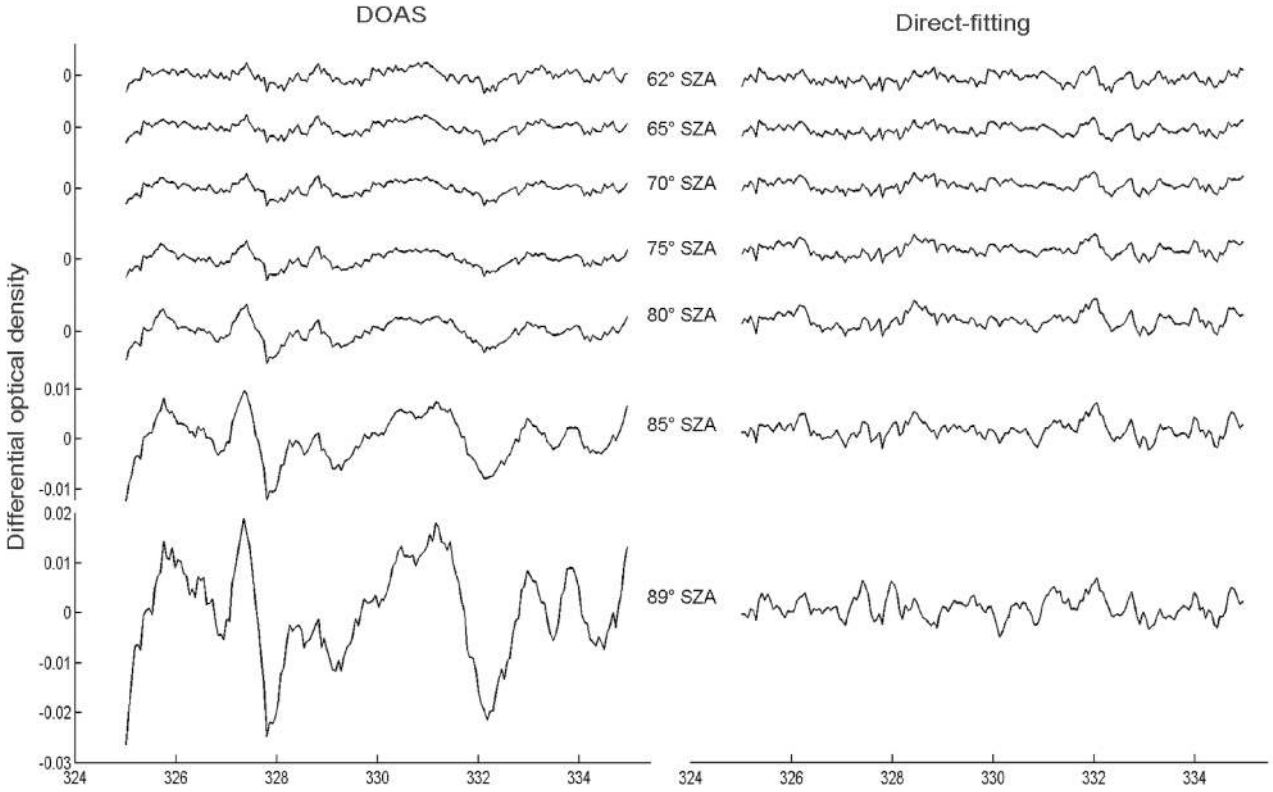

Figure 6. Comparison of total ozone fitting residuals obtained using the DOAS and direct-fitting retrieval schemes, for increasing values of the solar zenith angle. Poorly fitted ozone results typical of DOAS retrievals at low sun are strongly reduced with the direct-fitting approach.

as (logarithms) of the ratios of radiances with and without rotational Raman scattering (RRS). Amplitudes for Ring spectra (Fraunhofer and/or telluric) are regarded as ancillary DOAS fitting parameters; Ring interference is thus treated as "pseudo absorption." The simplest Ring spectrum is obtained by convolution of Raman cross-sections at a fixed temperature with a high-resolution Fraunhofer reference spectrum [*Chance and Spurr*, 1997]; this Ring spectrum is often sufficiently accurate for DOAS fitting of optically thin trace gas absorbers.

[67] The lack of a molecular Ring correction for earlier versions of GDP GOME total ozone retrieval was recognized as an important source of error [*Van Roozendael et al.*, 2002]. This was remedied in GDP4 and other algorithms [*Van Roozendael et al.*, 2006; *Eskes et al.*, 2005; *Coldewey-Egbers et al.*, 2005]. An improved semi-empirical Ring correction was also developed for total ozone direct-fitting, along with the related DOAS implementation in GDP4 [*Van Roozendael et al.*, 2006].

[68] The semi-empirical molecular Ring correction for GDP5 is based on a simplified RRS contribution to the intensity; referring to equation (13), the Ring spectrum is written:

$$S_{Ring}(\lambda) = I_0^{RRS}(\lambda) e^{-\tau_{O3}^{RRS}}. \tag{16}$$

[69] There are several approximations here. First, Raman light is assumed to be produced close to the surface, with a spectral shape given by a source spectrum for Raman scattering $I_0^{RRS}(\lambda)$. This source spectrum only treats the spectral smoothing effect of RRS on the solar intensity, and is determined by convolution of a GOME irradiance spectrum with Raman cross sections. The fractional intensity of Raman light (the E_{Ring} parameter) is freely adjustable; this may vary considerably and will depend on parameters such as cloud coverage, cloud altitude and surface albedo. Ozone absorption taking place in the incoming light is assumed to be fully smeared out in the inelastic process.

[70] The term τ_{O3}^{RRS} represents the effective optical density of ozone in the Raman light along the line-of-sight path from the surface to the satellite. To a first approximation, ozone absorption in the Raman light can be represented with sufficient accuracy by means of a simple geometrical enhancement factor (this is generally valid for a stratospheric absorber such as ozone):

$$\tau_{O3}^{RRS} = \tau_{O3}^{vertical} \sec\theta. \tag{17}$$

[71] Here, θ is the viewing zenith angle. We neglect the impact of incident beam ozone absorption before generation of Raman photons, since O_3 absorption structures are expected to be largely scrambled in the RRS process. The latter approximation is valid for most observations. However, for large solar zenith angles (>85°), ozone absorption in the incident beam is much stronger and its impact more noticeable. The following more accurate definition is then used:

$$\tau_{O3}^{RRS} = \tau_{O3}^{vertical} \left[\sec\theta + \Phi(O_0) \frac{\sigma_{O3}^{RRS}}{\sigma_{O3}} \right], \tag{18}$$

where $\Phi(\theta_0)$ is the geometrical enhancement factor of the incident beam (taking into account the Earth's sphericity) with θ_0 the solar zenith angle. Also, σ_{O3}^{RRS} is an ozone absorption cross-section for Raman scattering that is representative of ozone absorption after smoothing by RRS.

5.2. Cloud Preprocessing

[72] As with GDP4, we use the OCRA and ROCINN algorithms to provide ancillary cloud information (cloud fraction f_c, cloud top height h_c, and cloud top albedo A_c) in GDP5. The algorithms are described in more detail in the GDP4.0 paper [*Van Roozendael et al.*, 2006] and elsewhere, so the summaries here are brief. The FRESCO O_2 *A* Band least squares algorithm [*Koelemeijer and Stammes*, 2001; *Wang et al.*, 2008] was used in some GDP5 sensitivity studies.

[73] OCRA (Optical Cloud Recognition Algorithm) [*Loyola and Ruppert*, 1998] is an optical sensor cloud detection algorithm based on two components: a cloud-free background and a residual contribution. For GOME, OCRA uses the sub-pixel broadband reflectance as delivered by the polarization measurement devices (PMDs). Reflectances are mapped to normalized *rg*-color space and cloud-free pixels are selected according to a brightness criterion. The geometric cloud fraction is determined by examining separations between RGB reflectances and their cloud-free composite values. A detailed description is given by *Loyola* [2000].

[74] ROCINN [*Loyola*, 2004] takes the cloud fraction f_c derived from OCRA as input, and uses a neural network (NN) scheme to invert GOME reflectivities in and around the O_2 *A* band. ROCINN [*Loyola et al.*, 2006] retrieves height h_c and albedo A_c. For the NN inversion, ROCINN requires a complete data set of simulated reflectances for all viewing geometries and geophysical scenarios, and for various combinations of f_c, h_c and A_c. Reflectances in ROCINN 2.0 are calculated with the VLIDORT radiative transfer model [*Spurr*, 2006] including the effects of polarization and an exact treatment of single scattering in a curved atmosphere. For oxygen absorption, line spectroscopic information for the O_2 *A* band is taken from the HITRAN 2004 database [*Rothman et al.*, 2003]. Calculations are done at high resolution before convolution with the instrument function. Reflectances in the earlier ROCINN Version 1.0 were based only on O_2 *A* band absorption. The classification includes values of A_c as low as 0.3, with the highest h_c at 14 km, and the wavelength range optimized to 758–771 nm. ROCINN 2.0 was developed into a stand-alone library with flexible porting (tested on Intel and GNU compilers) and full documentation, and can process all GOME measurement types (nominal 1.5 or 6-s pixels, etc.).

[75] An initial verification of OCRA and ROCINN was described by *Van Roozendael et al.* [2006] using ATSR-2 data, obtained simultaneously with GOME (both instruments are on ERS-2). This ATSR-2 comparison confirmed the results reported by *Tuinder et al.* [2004] where several algorithms for retrieving cloud fraction using GOME data were compared against synoptic surface observations. An inter-comparison of GOME and ATSR cloud top heights was performed for the ROCINN and the SACURA algorithms [*Rozanov et al.*, 2006]. It was found that ROCINN was on average 0.5 km below ATSR, with SACURA 0.6 km above. Comparisons were restricted to high cloud-cover scenes. Cloud fractions from OCRA and MERIS were also compared [*Casadio et al.*, 2006]. MSG (Meteosat Second Generation)

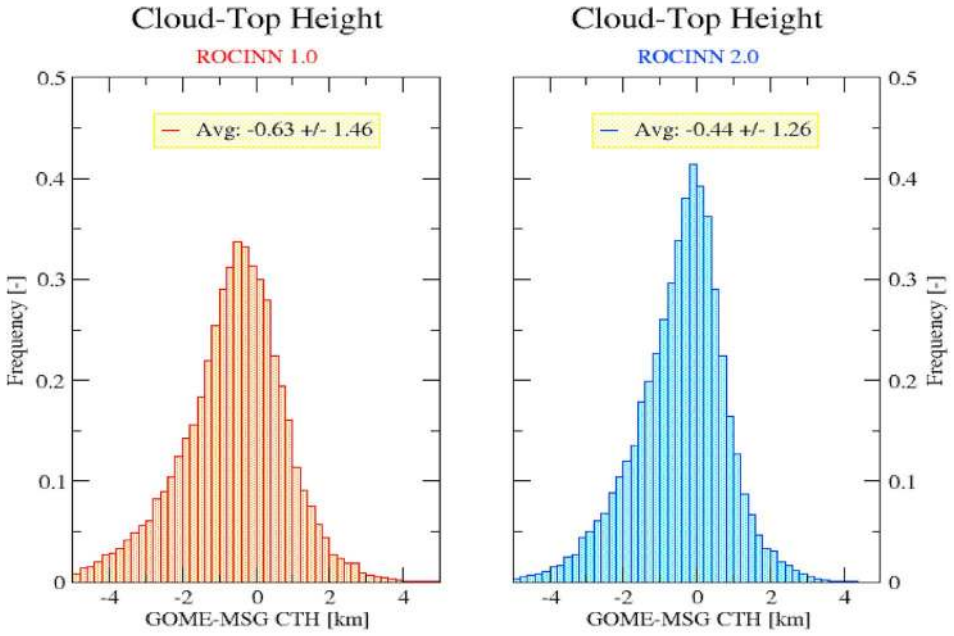

Figure 7. Cloud top height from ROCINN compared with Meteosat Second Generation (MSG) values; frequency histograms of height differences.

comparisons have been done with ROCINN Versions 1.0 and 2.0 [*Loyola et al.*, 2010]. Figure 7 is adapted from this work and clearly demonstrates the improvement in MSG validation to be gained with ROCINN Version 2.0.

6. Initial Results and Validation

[76] In the sequel paper (Lambert et al., manuscript in preparation, 2012), we give a detailed analysis of the validation campaign for the GDP5 algorithm as integrated in the UPAS operational system at DLR. There, comparisons of GDP5 total ozone against values from ground-based networks (GAW Brewer and Dobson, and NDACC UV-visible) are presented in detail, along with validations against total ozone products from other satellite instruments, namely, the OMI, SCIAMACHY and GOME-2 sensors. Comparisons with GOME ozone results from the previous GDP4 total ozone algorithm are also reported. The sequel paper also discusses validation methodology, including co-location criteria and selection of stations for the ground-based comparisons, and orbital coincidences for comparisons with other satellites. Here we provide a flavor of the new results, comparing the GDP5 record and other satellite data against ground based data, and looking at the stability of the time series. We also show individual-station results illustrating two improvements of GDP5 with respect to ground-based data: a reduced GOME SZA dependence and a smaller annual seasonality cycle.

[77] During the GDP4 validation work [*Balis et al.*, 2007a], it was shown that in general, the GDP4 algorithm provides an ozone record that is "accurate at the 1% level" for most regions and seasons for which the solar zenith angle (SZA) remains below 70 degrees. With the GDP5 record this excellent data quality remains, and even extends to larger solar zenith angles, as illustrated below.

[78] Another major feature of the GDP4 reprocessing was the remarkable time series stability of the 10-year GOME total ozone record from 1995 to 2005 [*Van Roozendael et al.*, 2006]. This stability is maintained with the new GDP5 algorithm: for the 16-year record (1995–2011), the long-term stability meets the requirement of 1%/decade at most validation stations. For instance, an 11-year time series of differences between GDP5 total ozone and Brewer measurements from Hohenpeissenberg (northern middle latitude site) showed an amplitude not larger than −0.4% and a drift of only −0.04%/year [*Lerot et al.*, 2010]. We may get an overview of the GDP5 record from Figure 8 which compares four satellite ozone records co-located against an ensemble of approximately 35 Brewer stations covering most of the Northern Hemisphere (from 20°N to 82.5°N). This ensemble has been utilized in similar validation studies (for details refer to *Balis et al.* [2007b]). The GOME GDP5 record shows no drift from 1996 onwards. Results are also shown for the SCIAMACHY ozone DOAS [*Lerot et al.*, 2010] SGP 3.01 record (from 2002), the OMI-DOAS [*Veefkind et al.*, 2006] v1.0.5 record (from 2005), and the OMI-TOMS [*Bhartia*, 2003] v8.5 record (from 2005). The GOME data quality is evident; note in particular the absence of bias in the GOME data, and the lower variability in the most recent years.

[79] Average solar zenith angle (SZA) dependence of historical GDP 3.0 ozone columns ranged from a few percent to ±10%, depending on the latitude, the season, and the ozone column [*Spurr et al.*, 2005]. Algorithm improvements in GDP4 resulted in a dramatic reduction of the SZA dependence, with remaining residual uncertainties of ±5% at SZA beyond 80°, inherent to the DOAS fitting approach. In the sequel paper, we will see that with GDP5 this SZA dependence has fallen to within ±1% up to 84° of SZA, and ±4% beyond this value. This reduction is observed at

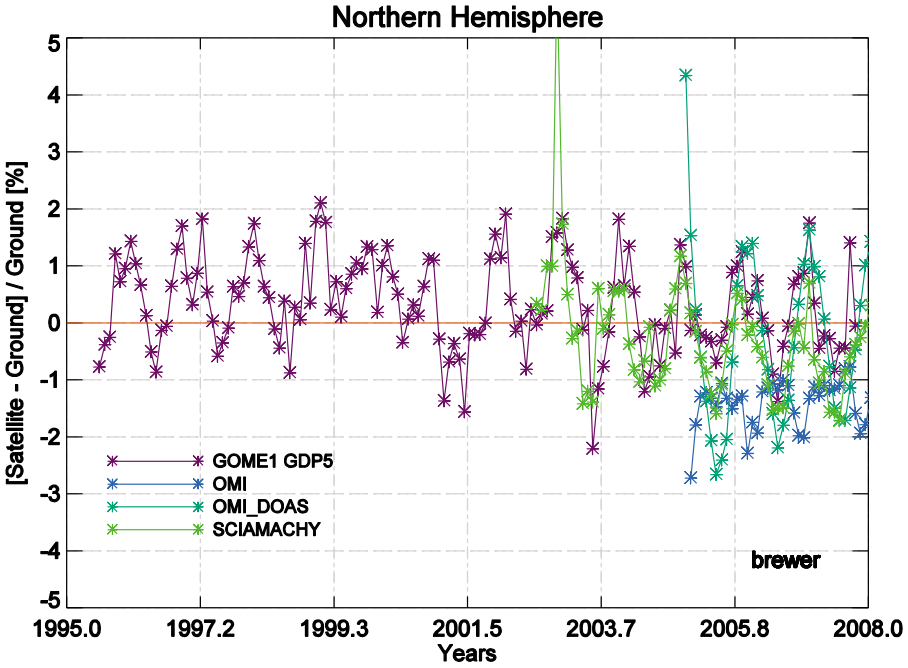

Figure 8. Comparisons of OMI-DOAS (cyan), OMI-TOMS (blue), SCIAMACHY (green) and GOME GDP5.0 (purple) data with ground-based data, for an ensemble of Brewer geolocations, showing time series of differences averaged over the Northern hemisphere.

individual stations as well as with global statistics, and is not a consequence of averaging the comparison results. Comparisons at middle and low latitude sites show no SZA dependence at low and moderate SZA values. In Figure 9, the absence of SZA dependence up to 84° is demonstrated at the Arctic station of Sodankylä for the four seasons. During the polar day, when GOME overpasses the same stations several times a day under different SZAs, there is no bias between GOME GDP5 data obtained in the mid morning (moderate SZA) and those obtained under midnight sun (large SZA).

[80] Finally we illustrate how GDP5 reduces (compared with GDP4) the seasonality cycle of total ozone differences with respect to the ground-based values. Figure 10 (taken from *Lerot et al.* [2010]) shows GDP4 and GDP5 validations against two Brewer stations in the northern hemisphere, namely, Hohenpeissenberg at middle latitudes and Sodankylä in the Arctic. In both cases, the residual cyclic (seasonal) signature is markedly improved, particularly for the Arctic station.

7. Concluding Remarks

[81] In this paper, we have described the new GDP5 algorithm for the direct fitting of total ozone from nadir UV satellite data. GDP5 derives from the original GODFIT algorithm co-developed at BIRA-IASB and has now been incorporated in the UPAS operational framework at DLR. The algorithm requires full radiative transfer simulations of radiances and Jacobians for total ozone and other retrieval parameters as part of a one-step least squares inversion. It has a new temperature-shifting process dealing with the temperature dependence of the ozone absorption cross-sections, and an internal albedo closure term. We have also summarized ancillary setups (empirical correction of the molecular Ring effect, preprocessing of cloud parameters).

[82] GDP5 is a stable algorithm with a higher level of accuracy than the DOAS-based GDP4 algorithm. It validates well against ground based ozone networks and also against results from the OMI satellite. Compared with GDP4, GDP5 ground-based comparisons show reduced biases and dependences on the season and the solar zenith angle, for nearly all regions. A thorough validation is reported in the sequel paper.

[83] In the past year, the GODFIT algorithm has been selected for the large-scale re-processing of the multi-year multiplatform total ozone data record, as part of the ESA Climate Change Initiative (CCI) Program. The present consortium of authors is now involved in extending and demonstrating the capability of the GOME direct-fitting algorithm to handle measurements from the SCIAMACHY instrument (since 2002) as well as GOME-2 on METOP-A (since October 2006), and later METOP-B (launch in 2012) and METOP-C (launch in 2017). Future missions such as GMES Sentinel-5 Precursor, Sentinel-4 and Sentinel-5 are also to be included in principle, providing a long-term data record of GOME-type accurate total ozone measurements [*Loyola et al.*, 2009] covering a time period of more than 35 years.

[84] The GDP5 total ozone and nitrogen dioxide data records covering the complete GOME mission from July 1995 will be released officially by ESA in spring 2012. The algorithm theoretical basis document (ATBD) (R. Spurr et al., GOME/ERS-2–GDP5.0 upgrade of the GOME data processor for improved total ozone columns–Algorithm theoretical basis document, 2011, http://atmos.caf.dlr.de/gome/docs/DLR_GOME_GDP5_ATBD.pdf), validation report and disclaimer (J.-C. Lambert et al., GOME/ERS-2–GDP5.0 upgrade of the GOME data processor for improved total ozone columns–Validation Report, 2011, http://atmos.caf.dlr.de/gome/docs/

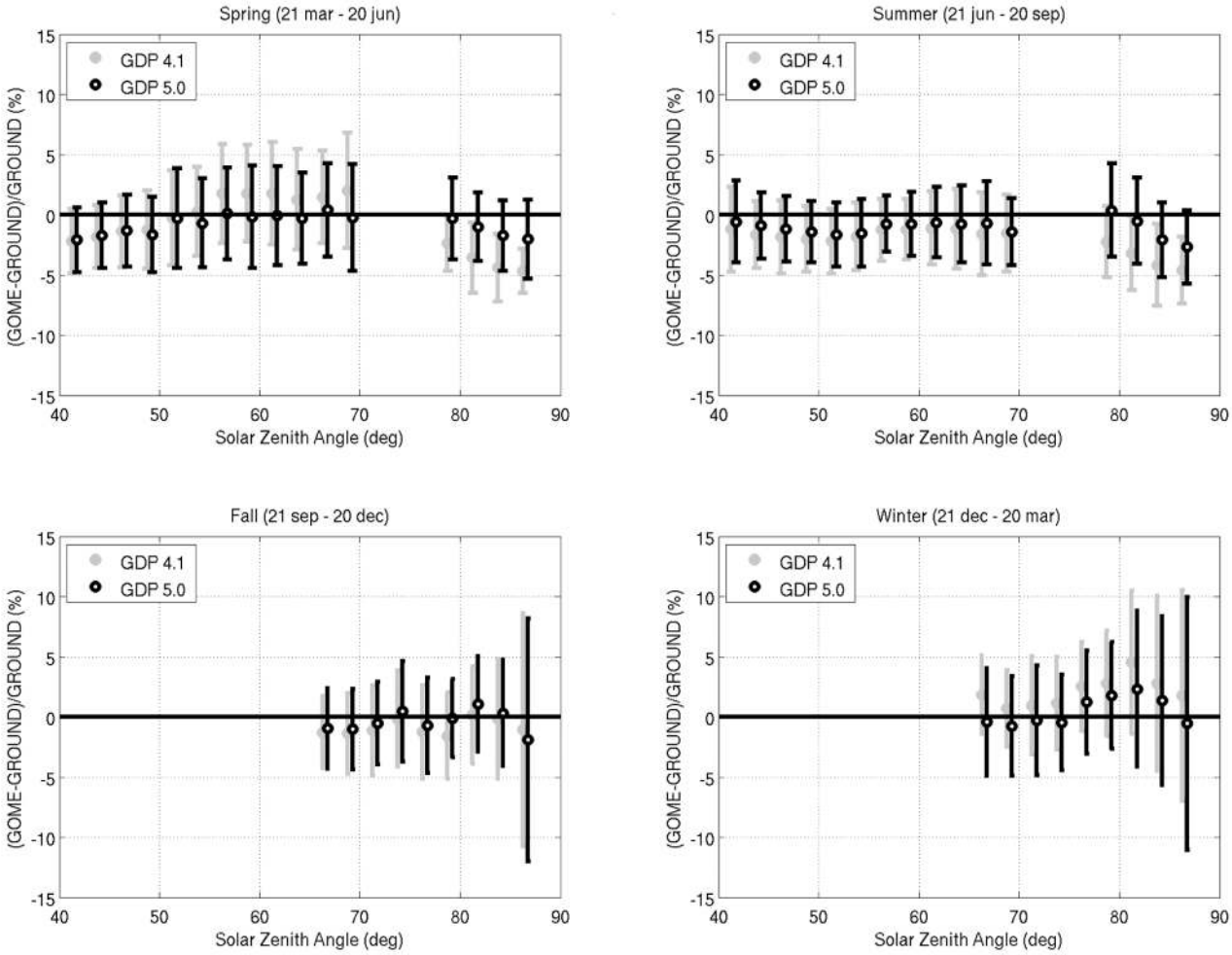

Figure 9. Mean and standard deviation of the relative difference between GOME (GDP 4.1 in gray and 5.0 in black) and ground-based total ozone from the Brewer operated by FMI-ARC in Sodankylä (Arctic Finland), plotted as a function of the GOME SZA, for the Spring, Summer, Fall and Winter seasons.

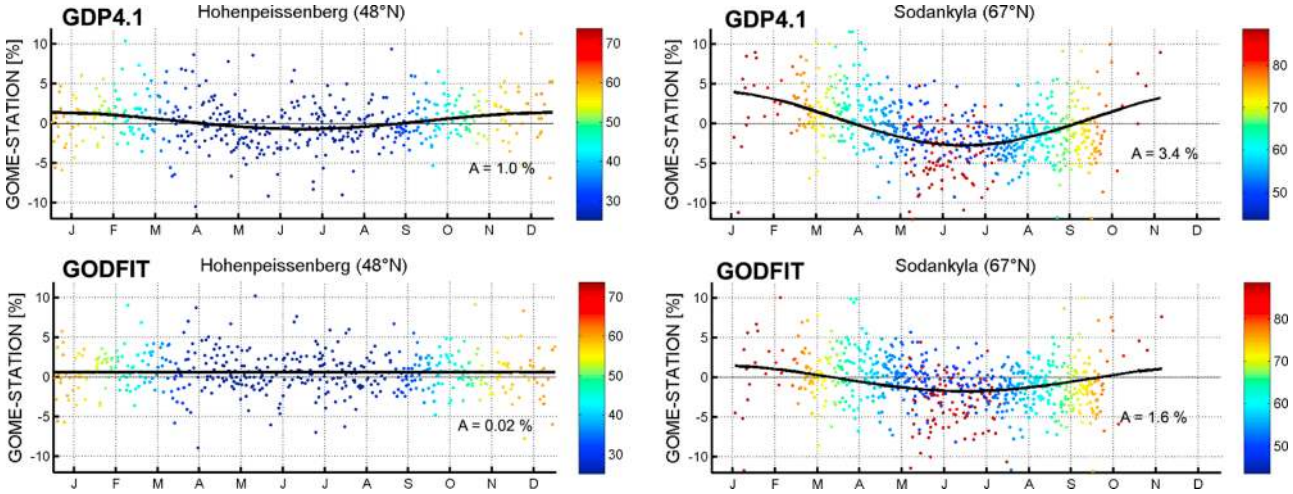

Figure 10. Seasonal variability for GODFIT (GDP5) and GDOAS (GDP4.1) total ozone validated against two northern hemisphere Brewer stations. Figure courtesy of *Lerot et al.* [2010].

BIRA_GOME_GDP5_VAL.pdf) and product user manual [*Loyola et al.*, 2011b] for GDP5 can be downloaded from the Website at http://atmos.caf.dlr.de/gome/documentation.html. The complete reprocessed GOME data record is available to the public at no cost via ftp server using a simple registration procedure through the ESA ESRIN - EO Help Desk at eohelp@esa.int. Images of the operational GOME trace gas and cloud products, a search engine and further information are available at http://atmos.caf.dlr.de/gome. Software to handle the GOME data is available at http://www.science-and-technology.nl/beat/.

[85] **Acknowledgments.** The authors are grateful to the European Space Agency (ESA-ESRIN) for their steadfast support for the entire project, from the GODFIT inception in 2003 through to the GDP5 reprocessing in 2011. Many scientists at a number of institutions in Europe and America have made contributions to the GOME data processing effort. In particular, we acknowledge colleagues from Uni. Bremen (Germany), KNMI (Netherlands), Uni. Heidelberg (Germany), BIRA-IASB (Belgium), DLR (Germany), SAO (USA), SRON (Netherlands), NASA Goddard (USA), RAL (Great Britain), AUTH (Greece) and EUMETSAT (Germany). The authors acknowledge ESA/DLR for provision of GOME level 1 products (see http://atmos.caf.dlr.de/gome) and ECMWF for provision of temperature profiles used in the algorithm development and testing. The ground-based data used for validation were obtained from the World Ozone and UV Data Centre (WOUDC) and the Network for the Detection of Atmospheric Composition Change (NDACC) and are publicly available (see http://woudc.org and http://ndacc.org). This work was funded through two ESA contracts: Upgrade of the GOME Data Processor for Improved Total Ozone Columns, ERSE-ESPR-EOPS-SW-04-0001; and Development of Algorithms for Retrieval of GOME Total Ozone Column, ESRIN contract 16403/02/I-LG. Validation and development work at BIRA-IASB was also supported in part by the Belgian PRODEX SECPEA project (PEA C90328).

References

Aliwell, S. R., et al. (2002), Analysis for BrO in zenith-sky spectra: An intercomparison exercise for analysis improvement, *J. Geophys. Res.*, *107*(D14), 4199, doi:10.1029/2001JD000329.

Balis, D., et al. (2007a), Ten years of GOME/ERS-2 total ozone data: The new GOME Data Processor (GDP) Version 4: II. Ground-based validation and comparisons with TOMS V7/V8, *J. Geophys. Res.*, *112*, D07307, doi:10.1029/2005JD006376.

Balis, D., M. Kroon, M. E. Koukouli, E. J. Brinksma, G. Labow, J. P. Veefkind, and R. D. McPeters (2007b), Validation of Ozone Monitoring Instrument total ozone column measurements using Brewer and Dobson spectrophotometer ground based observations, *J. Geophys. Res.*, *112*, D24S46, doi:10.1029/2007JD008796.

Bass, A., and R. Paur (1984), The ultraviolet cross sections of ozone: I. The measurements, in *Atmospheric Ozone, Proceedings of the Quadrennial Ozone Symposium*, edited by C. S. Zerefos and A. Ghazi, pp. 606–616, D. Reidel, New York.

Bhartia, P. (2003), Algorithm theoretical baseline document, TOMS v8 Total ozone algorithm, report, 23 pp., NASA Goddard Space Flight Cent., Greenbelt, Md. [Available at http://toms.gsfc.nasa.gov/version8/version8_update.html.]

Bodhaine, B., N. Wood, E. Dutton, and J. Slusser (1999), On Rayleigh optical depth calculations, *J. Atmos. Oceanic Technol.*, *16*, 1854–1861, doi:10.1175/1520-0426(1999)016<1854:ORODC>2.0.CO;2.

Boersma, K., H. Eskes, and E. Brinksma (2004), Error analysis for tropospheric NO_2 retrieval from space, *J. Geophys. Res.*, *109*, D04311, doi:10.1029/2003JD003962.

Bogumil, K., et al. (2003), Measurements of molecular absorption spectra with the SCIAMACHY Pre-Flight Model: Instrument characterization and reference data for atmospheric remote-sensing in the 230–2380 nm region, *J. Photochem. Photobiol. A*, *157*, 167–184, doi:10.1016/S1010-6030(03)00062-5.

Bovensmann, H., J. Burrows, M. Buchwitz, J. Frerick, S. Noel, V. Rozanov, K. Chance, and A. Goede (1999), SCIAMACHY: Mission objectives and measurement modes, *J. Atmos. Sci.*, *56*, 127–150, doi:10.1175/1520-0469(1999)056<0127:SMOAMM>2.0.CO;2.

Brion, J., A. Chakir, J. Charbonnier, D. Daumont, C. Parisse, and J. Malicet (1998), Absorption spectra measurements for the ozone molecule in the 350–830 nm region, *J. Atmos. Chem.*, *30*, 291–299, doi:10.1023/A:1006036924364.

Burrows, J., A. Richter, A. Dehn, B. Deters, S. Himmelmann, S. Voigt, and J. Orphal (1999), Atmospheric remote-sensing reference data from GOME: Part 2. Temperature-dependent absorption cross-sections of O_3 in the 231–794 nm range, *J. Quant. Spectrosc. Radiat. Transfer*, *61*, 509–517, doi:10.1016/S0022-4073(98)00037-5.

Casadio, S., D. Loyola, and C. Zehner (2006), GOME-MERIS cloud products inter-comparison on global scale, paper presented at Atmospheric Science Conference, Eur. Space Agency, Frascati, Italy.

Caudill, T., D. Flittner, B. Herman, O. Torres, and R. McPeters (1997), Evaluation of the pseudo-spherical approximation for backscattered ultraviolet radiances and ozone retrieval, *J. Geophys. Res.*, *102*, 3881–3890, doi:10.1029/96JD03266.

Ceccherini, S., and M. Ridolfi (2010), Technical Note: Variance-covariance matrix and averaging kernels for the Levenberg-Marquardt solution of the retrieval of atmospheric vertical profiles, *Atmos. Chem. Phys.*, *10*, 3131–3139, doi:10.5194/acp-10-3131-2010.

Chance, K., and R. L. Kurucz (2010), An improved high-resolution solar reference spectrum for Earth's atmosphere measurements in the ultraviolet, visible, and near infrared, *J. Quant. Spectrosc. Radiat. Transfer*, *111*, 1289–1295, doi:10.1016/j.jqsrt.2010.01.036.

Chance, K., and R. Spurr (1997), Ring effect studies: Rayleigh scattering including molecular parameters for rotational Raman scattering, and the Fraunhofer spectrum, *Appl. Opt.*, *36*, 5224–5230, doi:10.1364/AO.36.005224.

Chandrasekhar, S. (1960), *Radiative Transfer*, Dover, Mineola, N. Y.

Coldewey-Egbers, M., M. Weber, L. Lamsal, R. de Beek, M. Buchwitz, and J. Burrows (2005), Total ozone retrieval from GOME UV spectral data using the weighting function DOAS approach, *Atmos. Chem. Phys.*, *5*, 1015–1025, doi:10.5194/acp-5-1015-2005.

Daumont, D., J. Brion, J. Charbonnier, and J. Malicet (1992), Ozone UV spectroscopy. I. Absorption cross-sections at room temperature, *J. Atmos. Chem.*, *15*, 145–155, doi:10.1007/BF00053756.

Doicu, A., F. Schreier, and M. Hess (2004), Iterative regularization methods for atmospheric remote sensing, *J. Quant. Spectrosc. Radiat. Transfer*, *83*, 47–61, doi:10.1016/S0022-4073(02)00292-3.

Doicu, A., F. Schreier, S. Hilgers, A. von Bargen, S. Slijkhuis, M. Hess, and B. Aberle (2007), An efficient inversion algorithm for atmospheric remote sensing with application to UV limb observations, *J. Quant. Spectrosc. Radiat. Transfer*, *103*, 193–208, doi:10.1016/j.jqsrt.2006.05.007.

Eskes, H., R. van der A, E. Brinksma, J. Veefkind, J. de Haan, and P. Valks (2005), Retrieval and validation of ozone columns derived from measurements of SCIAMACHY on Envisat, *Atmos. Chem. Phys. Discuss.*, *5*, 4429–4475, doi:10.5194/acpd-5-4429-2005.

ETOP05 (1988), Digital relief of the surface of the Earth, *Data Announce. 88-MGG-02*, Natl. Geophys. Data Cent., NOAA, Boulder, Colo.

European Space Agency (ESA) (1995), GOME Global Ozone Monitoring Experiment users manual, edited by F. Bednarz, *ESA SP-1182*, 200 pp., Paris.

Grainger, J., and J. Ring (1962), Anomalous Fraunhofer line profiles, *Nature*, *193*, 762, doi:10.1038/193762a0.

Herman, J., and E. Celarier (1997), Earth surface reflectivity climatology at 340 nm to 380 nm from TOMS data, *J. Geophys. Res.*, *102*, 28,003–28,011, doi:10.1029/97JD02074.

Joiner, J., and P. Bhartia (1997), Accurate determination of total ozone using SBUV continuous spectral scan measurements, *J. Geophys. Res.*, *102*, 12,957–12,969, doi:10.1029/97JD00902.

Koelemeijer, R., and P. Stammes (2001), A fast method for retrieval of cloud parameters using oxygen *A* band measurements from the Global Ozone Monitoring Experiment, *J. Geophys. Res.*, *106*, 3475–3490, doi:10.1029/2000JD900657.

Koelemeijer, R., J. de Haan, J. Hovenier, and P. Stammes (2003), A database of spectral surface reflectivity in the range 335–772 nm derived from 5.5 years of GOME observations, *J. Geophys. Res.*, *108*(D2), 4070, doi:10.1029/2002JD002429.

Lambert, J.-C., et al. (2002), ERS-2 GOME GDP3.0 implementation and validation, edited by J.-C. Lambert, *ESA Tech. Note ERSE-DTEX-EOAD-TN-02-0006*, 139 pp., IASB, Brussels.

Lerot, C., M. Van Roozendael, J. van Geffen, J. van Gent, C. Fayt, R. Spurr, G. Lichtenberg, and A. von Bargen (2009), Six years of total ozone column measurements from SCIAMACHY nadir observations, *Atmos. Meas. Tech.*, *2*, 87–98, doi:10.5194/amt-2-87-2009.

Lerot, C., M. van Roozendael, J. van Gent, D. Loyola, and R. Spurr (2010), The GODFIT algorithm: A direct fitting approach to improve the accuracy of total ozone measurements from GOME, *Int. J. Remote Sens.*, *31*, 543–550, doi:10.1080/01431160902893576.

Levelt, P., G. van den Oord, M. Dobber, A. Malkki, H. Visser, J. de Vries, P. Stammes, J. Lundell, and H. Saari (2006), The Ozone Monitoring Instrument, *IEEE Trans. Geosci. Remote Sens.*, *44*, 1093–1101, doi:10.1109/TGRS.2006.872333.

Liu, X., M. Newchurch, R. Loughman, and P. K. Bhartia (2004), Errors resulting from assuming opaque Lambertian clouds in TOMS ozone retrieval, *J. Quant. Spectrosc. Radiat. Transfer*, *85*, 337–365, doi:10.1016/S0022-4073(03)00231-0.

Liu, X., K. Chance, C. Sioris, R. Spurr, T. Kurosu, R. Martin, and M. Newchurch (2005), Ozone profile and tropospheric ozone retrievals from Global Ozone Monitoring Experiment: Algorithm description and validation, *J. Geophys. Res.*, *110*, D20307, doi:10.1029/2005JD006240.

Liu, X., K. Chance, C. Sioris, and T. Kurosu (2007), Impact of using different ozone cross sections on ozone profile retrievals from Global Ozone Monitoring Experiment (GOME) ultraviolet measurements, *Atmos. Chem. Phys.*, *7*, 3571–3578, doi:10.5194/acp-7-3571-2007.

Loyola, D. (2000), Cloud retrieval for SCIAMACHY, paper presented at ERS-ENVISAT Symposium, Eur. Space Agency, Gothenburg, Sweden.

Loyola, D. (2004), Automatic cloud analysis from polar-orbiting satellites using neural network and data fusion techniques, paper presented at International Geoscience and Remote Sensing Symposium, IEEE, Anchorage, Alaska.

Loyola, D., and T. Ruppert (1998), A new PMD cloud-recognition algorithm for GOME, *ESA Earth Obs. Q.*, *58*, 45–47.

Loyola, D., et al. (1997), Ground segment for ERS-2 GOME data processor, *Eur. Space Agency Spec. Publ.*, *414*, 591–597.

Loyola, D., W. Thomas, Y. Livschitz, T. Ruppert, P. Albert, and R. Hollmann (2006), Cloud properties derived from GOME/ERS-2 backscatter data for trace gas retrieval, *IEEE Trans. Geosci. Remote Sens.*, *45*, 2747–2758.

Loyola, D., M. Coldewey-Egbers, M. Dameris, H. Garny, A. Stenke, M. Van Roozendael, C. Lerot, D. Balis, and M. Koukouli (2009), Global long-term monitoring of the ozone layer—A prerequisite for predictions, *Int. J. Remote Sens.*, *30*(15–16), 4295–4318, doi:10.1080/01431160902825016.

Loyola, D., W. Thomas, R. Spurr, and B. Mayer (2010), Global patterns in daytime cloud properties derived from GOME backscatter UV-VIS measurements, *Int. J. Remote Sens.*, *31*, 4295–4318, doi:10–1080/01431160903246741.

Loyola, D., et al. (2011a), The GOME-2 Total Column Ozone Product: Retrieval algorithm and ground-based validation, *J. Geophys. Res.*, *116*, D07302, doi:10.1029/2010JD014675.

Loyola, D., W. Zimmer, S. Kiemle, and P. Valks (2011b), Product User Manual for GOME total columns of ozone, NO_2, tropospheric NO_2, BrO, SO2, H_2O, HCHO, OClO, and cloud properties, *DLR/GOME/PUM/01*, 45 pp., DLR, Oberpfaffenhofen, Germany. [Available at http://atmos.caf.dlr.de/gome2/docs/DLR_GOME_PUM.pdf.]

Malicet, J., D. Daumont, J. Charbonnier, C. Parisse, A. Chakir, J. Brion, and U. V. Ozone (1995), Spectroscopy. II. Absorption cross-sections and temperature dependence, *J. Atmos. Chem.*, *21*, 263–273, doi:10.1007/BF00696758.

Munro, R., M. Eisinger, C. Anderson, J. Callies, E. Corpaccioli, R. Lang, A. Lefebvre, Y. Livschitz, and A. Perez Albinana (2006), GOME-2 on METOP: From in-orbit verification to routine operations, paper presented at Meteorological Satellite Conference, EUMETSAT, Helsinki.

Orphal, J. (2003), A critical review of the absorption cross-sections of O_3 and NO_2 in the 240–790 nm region, *J. Photochem. Photobiol. A*, *157*, 185–209, doi:10.1016/S1010-6030(03)00061-3.

Richter, A., and J. Burrows (2002), Tropospheric NO_2 from GOME measurements, *Adv. Space Res.*, *29*, 1673–1683, doi:10.1016/S0273-1177(02)00100-X.

Rothman, L., et al. (2003), The HITRAN molecular spectroscopic database: Edition of 2000 including updates through 2001, *J. Quant. Spectrosc. Radiat. Transfer*, *82*, 5–44, doi:10.1016/S0022-4073(03)00146-8.

Rozanov, A., V. Rozanov, and J. Burrows (2000), Combined differential-integral approach for the radiation field computation in a spherical shell atmosphere: Nonlimb geometry, *J. Geophys. Res.*, *105*, 22,937–22,942, doi:10.1029/2000JD900378.

Rozanov, A., A. Kokhanovsky, D. Loyola, R. Siddans, B. Latter, A. Stevens, and J. Burrows (2006), Intercomparison of cloud top altitudes as derived using GOME and ATSR-2 instruments onboard ERS-2, *Remote Sens. Environ.*, *102*, 186–193, doi:10.1016/j.rse.2006.02.009.

Slijkhuis, S., A. von Bargen, W. Thomas, and K. Chance (1999), Calculation of under-sampling correction spectra for DOAS spectral fitting, *ESA WPP-161*, pp. 563–569, Eur. Space Agency, Paris.

Slijkhuis, S., B. Aberle, and D. Loyola (2004), GOME data processor extraction software user's manual, *ER-SUM-DLR-GO-0045*, 50 pp., DLR, Oberpfaffenhofen, Germany.

Spurr, R. (2002), Simultaneous derivation of intensities and weighting functions in a general pseudo-spherical discrete ordinate radiative transfer treatment, *J. Quant. Spectrosc. Radiat. Transfer*, *75*, 129–175, doi:10.1016/S0022-4073(01)00245-X.

Spurr, R. (2003), LIDORT V2PLUS, a comprehensive radiative transfer package for nadir viewing spectrometers, *Proc. SPIE Int. Soc. Opt. Eng.*, *5235*, 89, doi:10.1117/12/511103.

Spurr, R. J. D. (2006), VLIDORT: A linearized pseudo-spherical vector discrete ordinate radiative transfer code for forward model and retrieval studies in multilayer multiple scattering media, *J. Quant. Spectrosc. Radiat. Transfer*, *102*, 316–342, doi:10.1016/j.jqsrt.2006.05.005.

Spurr, R. (2008), LIDORT and VLIDORT: Linearized pseudo-spherical scalar and vector discrete ordinate radiative transfer models for use in remote sensing retrieval problems, in *Light Scattering Reviews*, vol. 3, Part II, edited by A. Kokhanovsky, pp. 229–275, Springer, New York, doi:10.1007/978-3-540-48546-9_7.

Spurr, R., et al. (2005), GOME level 1-to-2 data processor version 3.0: A major upgrade of the GOME/ERS-2 total ozone retrieval algorithm, *Appl. Opt.*, *44*, 7196–7209, doi:10.1364/AO.44.007196.

Stamnes, K., S.-C. Tsay, W. Wiscombe, and K. Jayaweera (1988), Numerically stable algorithm for discrete ordinate method radiative transfer in multiple scattering and emitting layered media, *Appl. Opt.*, *27*, 2502–2509, doi:10.1364/AO.27.002502.

Stolarski, R. S., and S. Frith (2006), Search for evidence of trend slowdown in the long-term TOMS/SBUV total ozone data record: The importance of instrument drift uncertainty, *Atmos. Chem. Phys.*, *6*, 4057–4065, doi:10.5194/acp-6-4057-2006.

Tanskanen, A. (2004), Lambertian surface albedo climatology at 360 nm from TOMS data using moving time-window technique, paper presented at XX Quadrennial Ozone Symposium, Int. Ozone Comm., Kos, Greece.

Tanskanen, A., A. Arola, and J. Kujanpää (2003), Use of the moving time-window technique to determine surface albedo from the TOMS reflectivity data, *Proc. SPIE Int. Soc. Opt. Eng.*, *4896*, 239–250, doi:10.1117/12.483407.

Tuinder, O., R. de Winter-Sorkina, and P. Builtjes (2004), Retrieval methods of effective cloud cover for the GOME instrument: An intercomparison, *Atmos. Chem. Phys.*, *4*, 255–273, doi:10.5194/acp-4-255-2004.

van Oss, R., and R. Spurr (2002), Fast and accurate 4 and 6 stream linearized discrete ordinate radiative transfer models for ozone profile retrieval, *J. Quant. Spectrosc. Radiat. Transfer*, *75*, 177–220, doi:10.1016/S0022-4073(01)00246-1.

Van Roozendael, M., V. Soebijanta, C. Fayt, and J.-C. Lambert (2002), Investigation of DOAS issues affecting the accuracy of the GDP version 3.0 total ozone product, in *ERS-2 GOME GDP 3.0 Implementation and Delta Validation*, edited by J.-C. Lambert, *ERSE-DTEX-EOAD-TN-02–0006, ESA/ESRIN*, pp. 97–129, Eur. Space Agency, Frascati, Italy.

Van Roozendael, M., et al. (2006), Ten years of GOME/ERS-2 total ozone data: The new GOME Data Processor (GDP) version 4: 1. Algorithm description, *J. Geophys. Res.*, *111*, D14311, doi:10.1029/2005JD006375.

Veefkind, J. P., J. F. de Haan, E. J. Brinksma, M. Kroon, and P. F. Levelt (2006), Total ozone from the Ozone Monitoring Instrument (OMI) using the DOAS technique, *IEEE Trans. Geosci. Remote Sens.*, *44*(5), 1239–1244.

Wang, P., P. Stammes, R. van der A, G. Pinardi, and M. van Roozendael (2008), FRESCO+: An improved O_2 A-band cloud retrieval algorithm for tropospheric trace gas retrievals, *Atmos. Chem. Phys.*, *8*, 6565–6576, doi:10.5194/acp-8-6565-2008.

Weber, M., L. Lamsal, M. Coldewey-Egbers, K. Bramstedt, and J. Burrows (2005), Pole-to-pole validation of GOME WFDOAS total ozone with ground based data, *Atmos. Chem. Phys.*, *4*, 6909–6941.

Wellemeyer, C., S. Taylor, C. Seftor, R. McPeters, and P. Bhartia (1997), A correction for total ozone mapping spectrometer profile shape errors at high latitude, *J. Geophys. Res.*, *102*, 9029–9038, doi:10.1029/96JD03965.

D. Balis and M. Koukouli, Laboratory of Atmospheric Physics, School of Physics, Faculty of Sciences, Aristotle University of Thessaloniki, Box 149, GR-54124 Thessaloniki, Greece.

A. Doicu, D. Loyola, and W. Zimmer, Institut für Methodik der Fernerkundung, Deutsches Zentrum für Luft- und Raumfahrt, D-82234 Oberpfaffenhofen, Germany.

C. Fayt, J. Granville, J.-C. Lambert, C. Lerot, J. van Geffen, J. van Gent, and M. Van Roozendael, Belgian Institute for Space Aeronomy, 3 Ave. Circulaire, B-1180 Brussels, Belgium.

R. Spurr, RT Solutions, Inc., 9 Channing St., Cambridge, MA 02138, USA. (rtsolutions@verizon.net)

C. Zehner, ESRIN, ESA, Via Galileo Galilei CP.64, I-00044 Frascati, Italy.